International Journal of Earth Sciences
https://doi.org/10.1007/s00531-022-02214-0

ORIGINAL PAPER

Provenance of Oligocene–Miocene sedimentary rocks in the Cuu Long and Nam Con Son basins, Vietnam and early history of the Mekong River

H. Tim Breitfeld[1,2,3] · Juliane Hennig-Breitfeld[2,3] · Marcelle BouDagher-Fadel[4] · William J. Schmidt[5] · Kevin Meyer[6] · Jeff Reinprecht[6] · Terrence Lukie[6] · Trinh Xuan Cuong[7] · Robert Hall[2] · Nils Kollert[2] · Amy Gough[2] · Rafika Ismail[2]

Received: 14 February 2022 / Accepted: 27 May 2022

Abstract

The offshore Cuu Long (CLB) and Nam Con Son (NCSB) basins of SE Vietnam are two important Cenozoic hydrocarbon-bearing basins in the southern South China Sea (SCS), which can contribute to understanding the evolution of major SE Asian river systems, in particular the Mekong River. The Oligocene to Early Miocene basin fill of the Cuu Long Basin is dominated by sediment sourced locally from the Da Lat Zone basement on land. Sandstones have abundant Cretaceous detrital zircons and heavy mineral assemblages dominated by apatite and epidote. The Bach Ho Unconformity at c. 16 to 20.5 Ma marks a major provenance change and the overlying Middle to Late Miocene Con Son and Dong Nai formations were sourced by a large river system, which drained Indochina or even the Himalaya, resembling the present-day Mekong River. These formations have heterogeneous detrital zircon populations dominated by Triassic ages and zircon–rutile–tourmaline-dominated heavy mineral assemblages. The Oligocene Cau and Early Miocene Dua formations of the Nam Con Son Basin have a similar provenance to the CLB Con Son and Dong Nai formations, indicating a comparable drainage history of a large proto-Chao Phraya. At the Dua Unconformity at c. 15.4 to 17 Ma the Indochina provenance signature changes to a predominant Sibumasu signature.

The early Mekong River evolution is suggested to have involved two river systems. A proto-Mekong 1 initially filled the CLB, while at the same time a proto-Chao Phraya River with a capture area into the Himalaya filled the Malay Basin and/or the NCSB. At the end of the Early Miocene drainage was completely reorganised, and the proto-Mekong 1 captured the headwaters of the proto-Chao Phraya and became the proto-Mekong 2, while the NCSB was filled by sediment from the Malay–Thai Peninsula. This major change marks a very important drainage reorganisation in the southern SCS region.

Keywords Cuu Long Basin · Nam Con Son Basin · U–Pb geochronology · Provenance · Heavy minerals · Mekong River

✉ H. Tim Breitfeld
Tim.Breitfeld1@geo.tu-freiberg.de

1 Institut für Geologie, TU Bergakademie Freiberg, Bernhard-von-Cotta-Straße 2, 09599 Freiberg, Germany

2 SE Asia Research Group, Department of Earth Sciences, Royal Holloway University of London, Egham TW20 0EX, Surrey, UK

3 Chemostrat Ltd, Ravenscroft Court, Buttington Cross Enterprise Park, Welshpool, Powys SY21 8SL, UK

4 Department of Earth Sciences, University College London, London WC1H 0BT, UK

5 Vietnam Petroleum Institute, 167 Trung Kinh, Cau Giay, Hanoi, Viet Nam

6 Talisman Energy/Repsol Vietnam, Ho Chi Minh City, Viet Nam

7 PetroVietnam Group, PetroVietnam Tower, 18 Lang Ha, Dong Da, Hanoi, Viet Nam

Published online: 04 July 2022

Introduction

The Cenozoic basins of the South China Sea (SCS) margin have a long history of successful hydrocarbon exploration and production. Opening of the South China Sea in the Cenozoic, as well as sea level changes and hinterland uplift resulted in significant changes in depositional environments, input of clastic material and drainage into the basins. In the offshore region of SE Vietnam (Fig. 1) are the prolific Cuu Long (CLB) and Nam Con Son (NCSB) basins, which are the subject of this sediment provenance study.

Provenance studies in recent years around the South China Sea in NW Borneo, the Malay–Thai Peninsula, the Pearl River Basin in SE China, Palawan and the Philippines have revealed paleo-river courses, source areas for basin fills and helped to reconstruct tectonic evolution (e.g., Sevastjanova et al. 2011; van Hattum et al. 2013; Suggate et al. 2014; Liu et al. 2016; Galin et al. 2017; Basori et al. 2018; Breitfeld and Hall 2018; Wang et al. 2018; Yan et al. 2018; Dodd et al. 2019; Hennig-Breitfeld et al. 2019; Breitfeld et al. 2020a; Tang et al. 2020; Burley et al. 2021; Gong et al. 2021; Quek et al. 2021). The Yinggehai–Song Hong Basin in the Gulf of Tonkin (Fig. 1) has so far provided the most detailed provenance data from offshore Vietnam (e.g., Wang et al. 2014, 2019; Cao et al. 2015; Jiang et al. 2015; Fyhn et al. 2019). However, up to now the offshore region of SE Vietnam has been little studied due to limited sample availability, with the exception of preliminary provenance data from the Cuu Long Basin (Hennig et al. 2017a).

The Cuu Long and Nam Con Son basins are close to the SE Vietnam coast and the present-day Mekong River supplies sediment to the southern Cuu Long Basin (Fig. 1). The Mekong is the sixth longest river in Asia (Liu et al. 2009) and is very important for agriculture, climate and human development. Provenance studies of Cenozoic successions can help to understand the evolution of the Mekong River system by identifying the history of sediment deposition, uplift of source regions, changes of river courses, and provide insights into causes, such as tectonics and climate change. The objective of this study was to investigate the provenance of Oligocene to Late Miocene clastic sedimentary rocks offshore SE Vietnam to reconstruct the drainage history of major rivers in Indochina. We present here new heavy mineral data and detrital zircon geochronology based on samples from wells in the Cuu Long and Nam Con

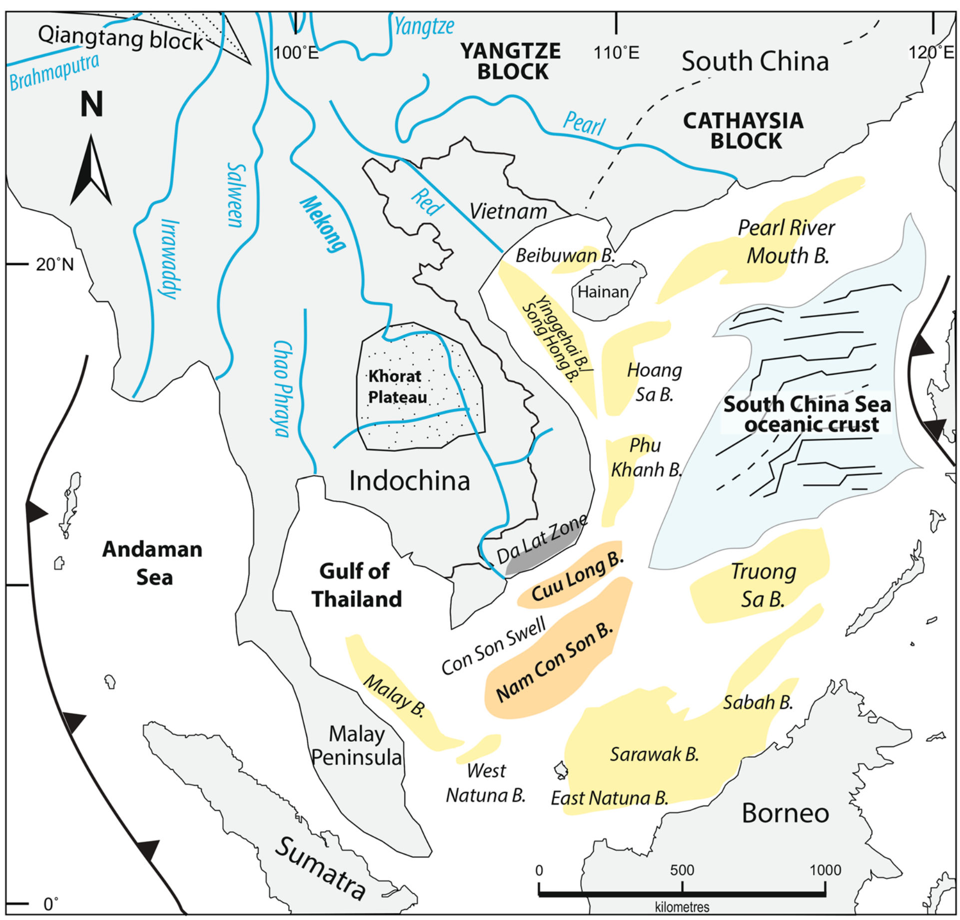

Fig. 1 Location of major Cenozoic sedimentary basins in the South China Sea region (modified from Clift et al. 2006; Hennig et al. 2018). The study area includes the Cuu Long and Nam Con Son basins (orange coloured) offshore SE Vietnam. Other important SCS basins coloured in yellow. The Da Lat Zone in SE Vietnam (Cretaceous granitoids) is coloured in dark grey as important proximal source region

Son basins to analyse river course and provenance changes. These are the first provenance data from these two basins. The results demonstrate that there is a major provenance change in the Cuu Long Basin in the Early Miocene from a proximal Da Lat Zone source to a wider Indochina source, which we interpret as reflecting the evolution of the proto-Mekong River. At around the same time in the Nam Con Son Basin there was a change from an Indochina to an Indochina–Sibumasu source, indicating a change in hinterland supply and drainage.

Regional background

The Sunda Shelf region includes several Cenozoic sedimentary basins that began to extend in the Late Eocene (Hall and Morley 2004). Rifting along the Sunda Shelf mostly ceased or paused when oceanic spreading began in the South China Sea at the Eocene–Oligocene boundary (Barckhausen et al. 2014; Larsen et al. 2018; Zhong et al. 2018), which continued until c. 15 or 16 Ma (Chang et al. 2015; Yu et al. 2018; Zhang et al. 2018; Zhong et al. 2018). Franke et al. (2014) identified two important unconformities in the South China Sea margins, the rift-onset unconformity and the end-rift or break-up unconformity with diachronous character and Paleocene to Eocene and Oligocene ages, respectively. The Cuu Long and Nam Con Son basins are two NE–SW trending basins in offshore SE Vietnam that are separated by the Con Son Swell. The basins contain Late Eocene/Oligocene to Miocene sediments that were deposited in fluvial to marine environments, which have been documented by 2D/3D seismic, wireline logs, biostratigraphy, palynology, and core petrography (e.g., Nguyen and Nguyen 1995; Matthews et al. 1997; Dien et al. 1998; Lee et al. 2001; Morley et al. 2011, 2019; Dung et al. 2018). These sediments were deposited above Mesozoic meta-sedimentary, metamorphic and igneous rocks that form the basement (e.g., Matthews et al. 1997; Cuong and Warren 2009). Figure 2 displays the Cenozoic stratigraphy of onshore and offshore SE Vietnam. Despite their close spatial relationship and similar sediment fill, the basins differ in their structure and evolution (e.g., Lee et al. 2001; Schmidt et al. 2019). Onshore, the Da Lat Zone in SE Vietnam consists predominantly of Cretaceous granitoids intruded into Triassic and Jurassic meta-sedimentary and

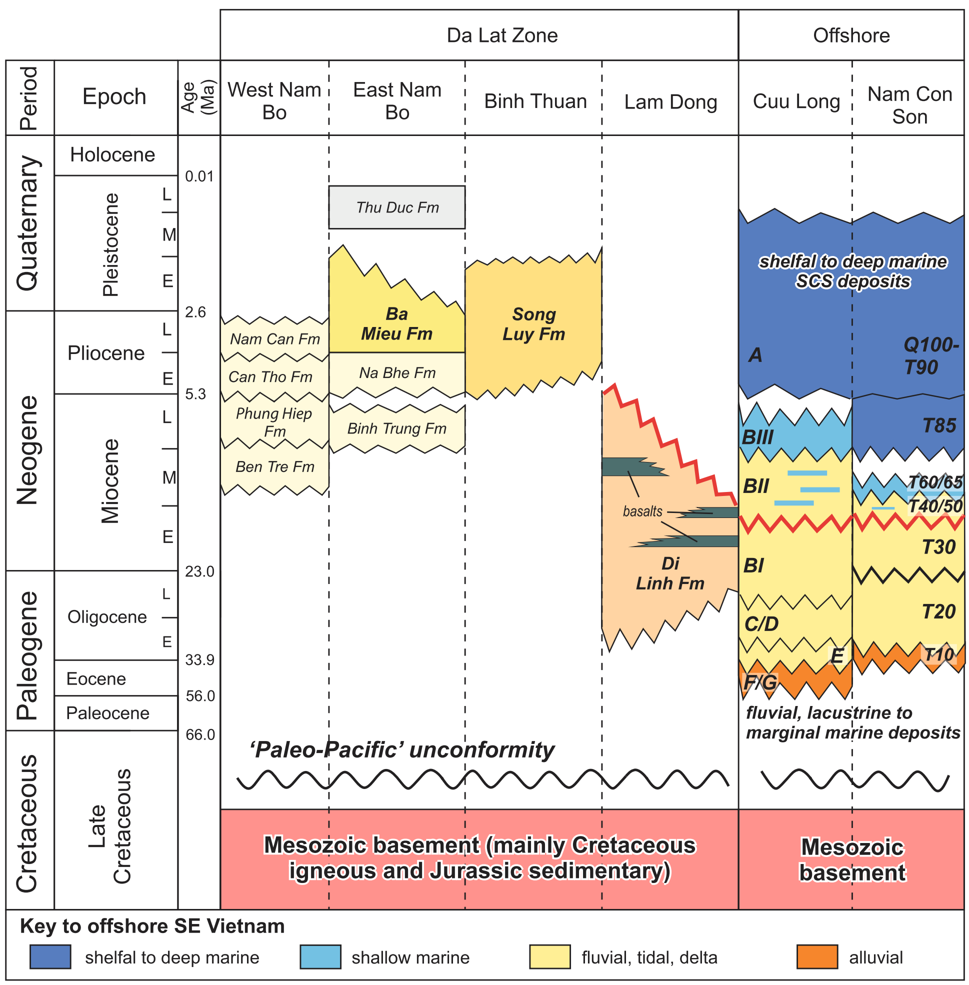

Fig. 2 Stratigraphic overview of the offshore successions in the Cuu Long and Nam Con Son basins and their time equivalents in onshore southern Vietnam (modified from Hennig et al. 2018). Letters in the CLB and NCSB represent the seismic horizons

Triassic igneous rocks (Nguyen et al. 2004; Fyhn et al. 2010; Shellnutt et al. 2013; Hennig-Breitfeld et al. 2021; Schmidt et al. 2021). This Cretaceous granitic belt extends into SW Vietnam and SE Cambodia (Fyhn et al. 2016; Nong et al. 2021; Waight et al. 2021) and across the Sunda Shelf into Borneo (Hennig et al. 2017b; Breitfeld et al. 2017, 2020b). The Cretaceous granites and volcanics in the Da Lat Zone are overlain by mainly fluvial to marginal marine Cenozoic sediments (Fig. 2). Hennig et al. (2018) presented heavy mineral and detrital zircon age provenance data for the Di Linh, Ba Mieu and Song Luy formations in the Da Lat Zone, which were probably largely eroded in the Pleistocene to Quaternary.

The Cuu Long Basin formed in the Cenozoic and is filled with c. 6 to 10 km of sediments (Lee et al. 2001; Cuong and Warren 2009; Fyhn et al. 2009; Schmidt et al. 2019) and has a history which includes rifting, inversion/compression, and thermal subsidence. Rifting initiated in the Eocene and continued until the end of the Oligocene (Lee et al. 2001; Schmidt et al. 2003; Hung and Le 2004; Fyhn et al. 2009) or the Early Miocene (Cuong and Warren 2009). Nguyen et al. (2019) documented two rift periods, a main phase from the Middle Eocene to the Oligocene and a late phase in the Early Miocene. This was followed by an episode of compression in the late Oligocene to Early Miocene (Schmidt et al. 2003, 2019; Hung and Le 2004; Cuong and Warren 2009; Fyhn et al. 2009). Schmidt et al. (2019) suggested rifting ceased in the mid-Oligocene, followed by inversion in the late Oligocene. The last stage of basin evolution is interpreted as a thermal sag phase beginning in the Early Miocene (Lee et al. 2001; Fyhn et al. 2009) or Middle Miocene (Cuong and Warren 2009; Nguyen et al. 2019). Schmidt et al. (2019) noted that none of the faults in the Mekong Delta Fault Zone or in the Cuu Long Basin cut significantly into the adjacent Con Son Swell or into the Nam Con Son Basin.

The Nam Con Son Basin is a Cenozoic rift basin that has been interpreted to be directly associated with the rifting and seafloor spreading of the South China Sea (East Vietnam Sea in Vietnamese literature) (Briais et al. 1993; Fyhn et al. 2009; Franke et al. 2014), although the South China Sea extension estimates of Hayes and Nissen (2005) cast doubt on how much influence spreading had on the SE Vietnam basins. Rifting of the Nam Con Son Basin started at c. 32 Ma (Swiecicki and Maynard 2009), later than many other basins across the Sunda region, where an earlier Eocene rift phase is commonly identified (Morley et al. 2011). Four principal megasequences based on tectonic stages of the Nam Con Son Basin have been identified and include syn-rift 1, inter-rift or post-rift 1, syn-rift 2 and post-rift 2 (Matthews et al. 1997; Lee et al. 2001; Morley et al. 2011; Meyer 2012; Tuan and Tri 2016; Dung et al. 2018). The megasequences are further subdivided into sequence stratigraphic third-order depositional sequences (T10 to Q100) that are correlated with lithostratigraphic units. The syn-rift 1 consists of sequence T10 deposited in the early Oligocene (Morley et al. 2011), possibly ranging down into the Late Eocene (Matthews et al. 1997; Dung et al. 2018). Inter-rift consists of T20 and T30 associated with regional subsidence possible in response to opening of the South China Sea. Syn-rift phase 2 includes sequences T40, T50, T60 and T65. This phase was followed by a regional uplift event in the Middle Miocene associated with major erosion, resulting in a regional Middle Miocene Unconformity (Matthews et al. 1997; Lee et al. 2001; Fyhn et al. 2009; Swiecicki and Maynard 2009; Morley et al. 2011; Tuan and Tri 2016; Dung et al. 2018). Following the inversion widespread subsidence resulted in deposition of post-rift 2 sequences T85 to Q100, which includes Plio-Pleistocene delta sediments that were interpreted as the prograding paleo-Mekong delta (Matthews et al. 1997; Morley et al. 2011; Tuan and Tri 2016).

Cuu Long Basin stratigraphy

The stratigraphy of the Cuu Long Basin is subdivided by seismic horizons labelled from Group F/G at the base to A at the top (e.g., Dien et al. 1998; Hung and Le 2004) (Fig. 3). The basement of the basin is predominantly formed by Cretaceous granites, with minor Late Triassic and Late Jurassic igneous rocks (Cuong and Warren 2009). Hennig-Breitfeld et al. (2021) reported a U–Pb zircon age of c. 90–92 Ma for the Cretaceous granite basement and concluded that it was the equivalent of the onshore Da Lat Zone Deo Ca Suite granites. The Bach Ho granite within the basin was dated by Nong et al. (2021) with zircon U–Pb as c. 110 Ma, more similar in age to the onshore Dinh Quan suite (Hennig-Breitfeld et al. 2021). The Con Dao Island granite southwest of the Cuu Long Basin was dated by Nong et al. (2021) as c. 83 Ma, similar to the onshore Ankroet suite (Hennig-Breitfeld et al. 2021). This suggests that the Cretaceous basement of the Cuu Long Basin is formed by different Cretaceous granitoids similar to the onshore Da Lat Zone. The sedimentary successions of the Cuu Long Basin begin locally with the Eocene Ca Coi Formation (seismic groups F and G) and the more widespread Late Eocene to early Oligocene Tra Cu Formation (seismic group E) (Hung and Le 2004; San et al. 2013; Quang 2013; Morley et al. 2019). These formations consist of alluvial, fluvial and lacustrine fine to coarse grained sandstones interbedded with conglomerates, and siltstones, minor mudstones and thin coals (Cuong and Warren 2009; Morley et al. 2019). They are unconformably overlain by the Tra Tan Formation (seismic groups C and D) (Morley et al. 2019). Depositional environments range from fluvial and lacustrine to brackish and intertidal with some interbedded volcaniclastics (Hung and Le 2004; Cuong and Warren 2009; San et al. 2013; Morley et al. 2019). An early Oligocene age is interpreted for the formation by Morley

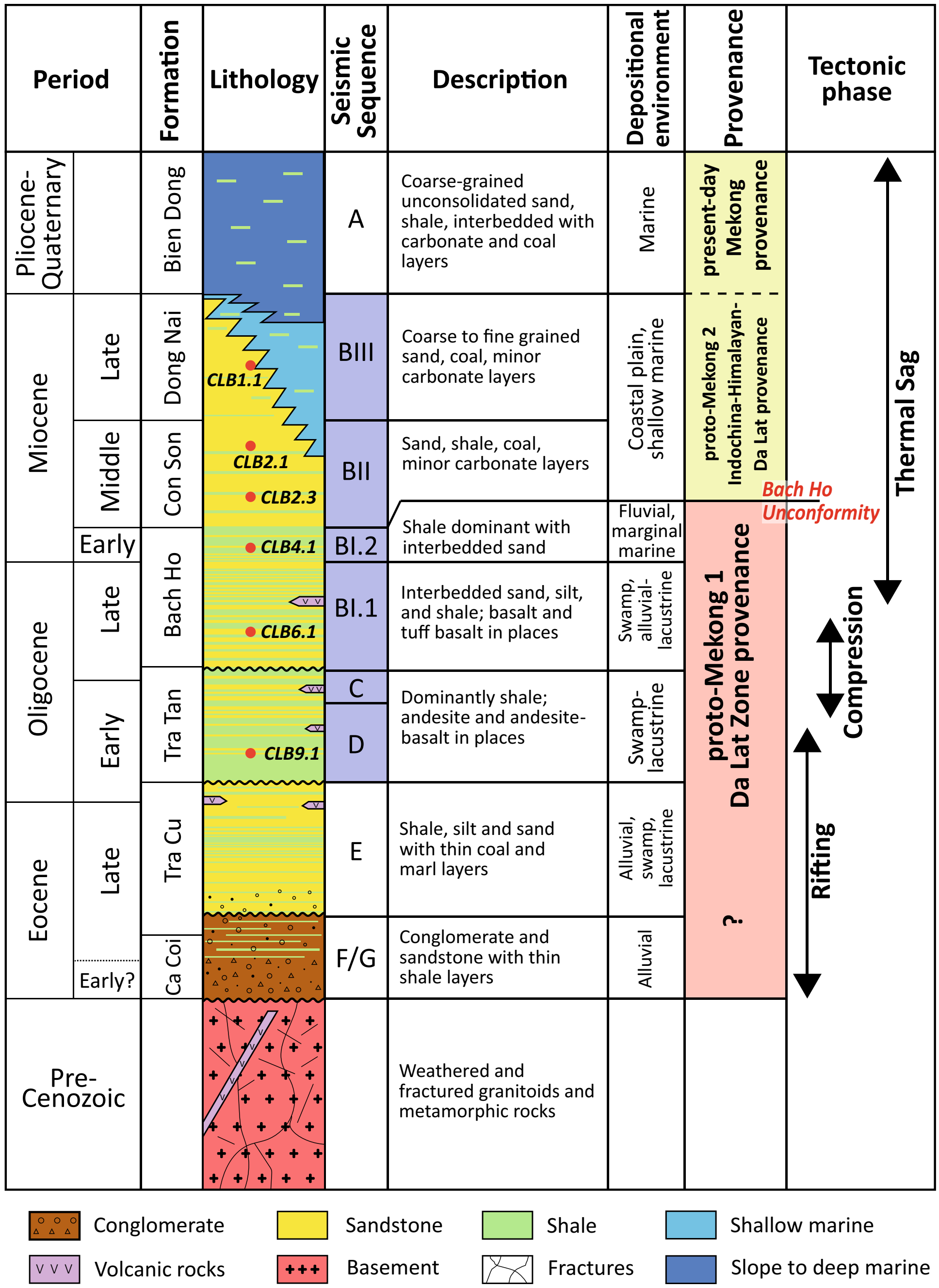

Fig. 3 Stratigraphy of the Cuu Long Basin with depositional environments, tectonic phases, and provenance signature (modified from Tran and Phung 2007; Morley et al. 2019; Schmidt et al. 2019), displaying schematically the sample positions (red dots). Seismic sequences D to BIII (Tra Tan Formation to Dong Nai Formation) were analysed in this study

et al. (2019) in contrast to the previous Oligocene or late Oligocene interpretation (e.g., Cuong and Warren 2009). The formation is subdivided into Lower (seismic group D) and Upper (seismic group C) parts separated by an unconformity (Morley et al. 2019). The Bach Ho Formation (seismic group BI.1 and BI.2) unconformably overlies the Tra Tan Formation and consists mainly of shallow marine shales and sands, and some mudstones with strong deltaic and fluvial influence (Cuong and Warren 2009; Morley et al. 2019). The formation was interpreted to be Early Miocene (e.g., Cuong and Warren 2009), but Morley et al. (2019) revised the age to mainly late Oligocene for the Lower Member (BI.1) and Early Miocene for the Upper Member (BI.2) based on the occurrence of a *Rotalia* shale with common *Ammonia* spp. in the upper part. An unconformity is interpreted between the two members at the Oligocene–Miocene boundary (Morley et al. 2019). The Middle Miocene Con Son Formation (seismic group BII) unconformably overlies the Bach Ho Formation and is dominated by coastal to fluvial deposits and interpreted (Cuong and Warren 2009; Morley et al. 2019). Unconformably on top is the Late Miocene Dong Nai Formation (seismic group BIII), which consists of shallow

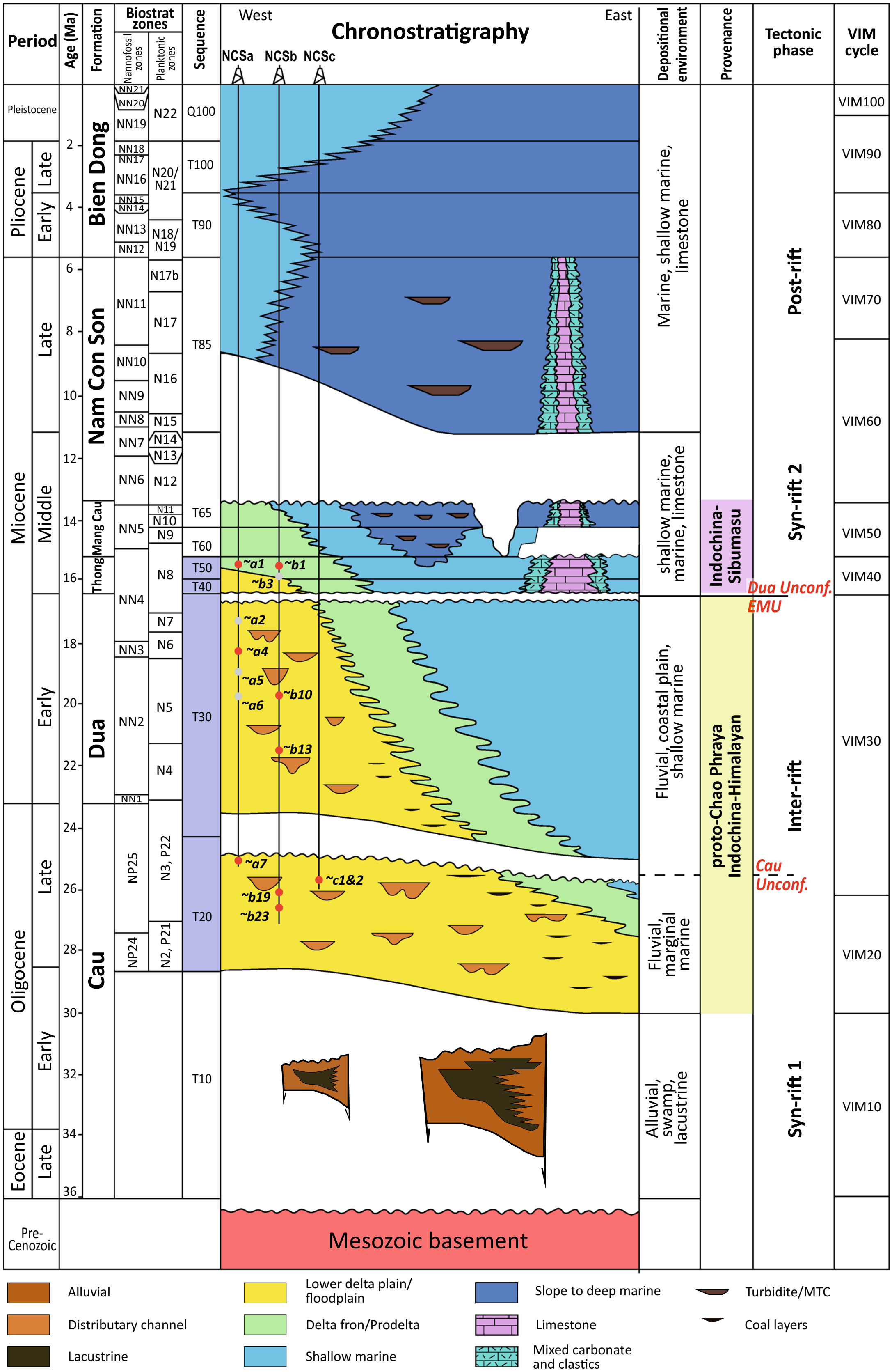

Period
Age (Ma)
Formation
Biostrat zones
Nannofossil zones
Planktonic zones
Sequence
West
Chronostratigraphy
East
NCSa NCSb NCSc
Depositional environment
Provenance
Tectonic phase
VIM cycle
Pleistocene
Pliocene
Miocene
Oligocene
Eocene
Pre-Cenozoic
Late
Early
Middle
Bien Dong
Nam Con Son
Thong
Mang Cau
Dua
Cau
Q100
T100
T90
T85
T65
T60
T50
T40
T30
T20
T10
~a1
~b1
~b3
~a2
~a4
~a5
~b10
~a6
~b13
~a7
~c1&2
~b19
~b23
Mesozoic basement
Marine, shallow marine, limestone
shallow marine, marine, limestone
Fluvial, coastal plain, shallow marine
Fluvial, marginal marine
Alluvial, swamp, lacustrine
Indochina-Sibumasu
proto-Chao Phraya Indochina-Himalayan
Post-rift
Syn-rift 2
Inter-rift
Syn-rift 1
Dua Unconf.
EMU
Cau Unconf.
VIM100
VIM90
VIM80
VIM70
VIM60
VIM50
VIM40
VIM30
VIM20
VIM10
Alluvial
Distributary channel
Lacustrine
Lower delta plain/ floodplain
Delta fron/Prodelta
Shallow marine
Slope to deep marine
Limestone
Mixed carbonate and clastics
Turbidite/MTC
Coal layers

◂**Fig. 4** Stratigraphy of the Nam Con Son Basin with depositional environments, tectonic phases, and provenance signature (modified from Dung et al. 2018). Seismic sequences T20 to T40&50 (Cau to Thong Formation) were analysed in this study. Display of the three analysed wells (NCSa, NCSb and NCSc) and position of the samples is only schematically. Red dots include heavy mineral and detrital zircon geochronology samples. Grey dots comprise biostratigraphy samples

marine, river mouth and coastal deposits (Cuong and Warren 2009; Morley et al. 2019). The youngest formation is the Pliocene to Quaternary Bien Dong Formation (seismic group A), which is dominated by open marine fine-grained sediments deposited in a shelfal environment (Cuong and Warren 2009).

Nam Con Son Basin stratigraphy

The Nam Con Son Basin is subdivided into seismic sequences labelled from T10 (Late Eocene to early Oligocene) to Q100 (Pleistocene) corresponding to various lithostratigraphic units (Fig. 4) (Matthews et al. 1997). Based on the seismic sequences, Morley et al. (2011) introduced sequence biostratigraphy cycles VIM (Vietnam/Indonesia/Malaysia) and revised the ages for the corresponding formations. Therefore, the seismic sequences of Matthews et al. (1997) do not correspond exactly to the lithostratigraphic formations (Morley et al. 2011). The basement is formed by granitic, volcanic and metasedimentary rocks (Matthews et al. 1997), from which volcanic rocks have been dated by zircon U–Pb as 200.4 ± 1.6 Ma (Hennig-Breitfeld et al. 2021). Cretaceous granitoids have also been reported by the K-Ar method (Hutchison 1989; Areshev et al. 1992). Above the basement T10 and VIM10 forms the first sedimentary package consisting of alluvial fan/fluvial to lacustrine deposits, and is assumed to be Late Eocene to early Oligocene (Matthews et al. 1997; Morley et al. 2011; Dung et al. 2018). The T10 sequence has not been penetrated anywhere in the basin, and its age must be inferred from the overlying T20 sequence. The T10 seismic sequence corresponds to the Tien Cau Formation (Morley et al. 2011). T20 and VIM20 is dominated by fluvial sandstones overlain by coals, mudstones and thinner sandstone packages and interpreted as backstepping fluvio-deltaic facies with minimal tidal influence (Matthews et al. 1997; Morley et al. 2011). VIM20 corresponds to the Cau Formation and is dated as late Oligocene (Bat et al. 1993; Matthews et al. 1997). Nguyen and Nguyen (1995) report a thickness of 200 to 800 m for the Cau Formation. T30 and VIM30 unconformably above are interpreted as late Oligocene to Early Miocene transgressive sandstones and marine mudstones overlain by interbedded sandstones and mudstones (Matthews et al. 1997; Morley et al. 2011; Dung et al. 2018). They are fluvial, estuarine and brackish shoreface deposits with occasional intercalations of more open marine sediments (Matthews et al. 1997). T30 and VIM30 correspond to the Dua Formation (Bat et al. 1993; Nguyen and Nguyen 1995; Matthews et al. 1997; Morley et al. 2011). Nguyen and Nguyen (1995) report a thickness from 200 m to over 1000 m. Tham and Su (2016) reported Early Miocene calcareous nannofossils (zones NN2 to NN4). Seismic sequence T40 and VIM40 is interpreted to be unconformably above with a shift from the predominantly paralic facies of T30 to shelfal marine clastic sediments and carbonates of T40 (Matthews et al. 1997). The sequences correspond to the Thong Formation and are dated as late Early Miocene to early Middle Miocene (Bat et al. 1993; Matthews et al. 1997; Morley et al. 2011; Dung et al. 2018). The Thong Formation also includes seismic sequence T50 (Dung et al. 2018). The Middle Miocene T60 and T65 are dominated by shelfal sediments and deep water clastic sediments (Matthews et al. 1997). They correspond to the Mang Cau Formation (Bat et al. 1993; Nguyen and Nguyen 1995; Matthews et al. 1997; Dung et al. 2018), and to cycle VIM50 (Morley et al. 2011). The top of the sequence is a prominent unconformity marking a basinward shift of deep water sedimentation and mild inversion of the underlying successions (Matthews et al. 1997). T80 and T85 are unconformably above T65 and comprise Late Miocene deposits (Matthews et al. 1997). They correspond broadly with the VIM70 cycle (Morley et al. 2011). The lower part (T80) is dominated by widespread shelf carbonates with restricted shallow water clastics and deep water mudstones between the build-ups (Matthews et al. 1997). The upper part (T85) is composed of shelf and slope clastic deposits with some restricted carbonate facies, and turbidite facies (Matthews et al. 1997). The Nam Con Son Formation is the lithostratigraphic equivalent (Bat et al. 1993; Matthews et al. 1997). Sequences T90, T100 and Q100 correspond to the Bien Dong Formation and broadly to VIM cycles 80, 90 and 100, and range from the Early Pliocene to the Pleistocene with mostly shelfal, slope and deep water deposits (Bat et al. 1993; Matthews et al. 1997; Morley et al. 2011; Dung et al. 2018) and delta deposits (Morley et al. 2011).

Methodology

Sampling

Samples were provided from wells in the Cuu Long and Nam Con Son basins by Talisman Vietnam (now Repsol Vietnam) in cooperation with the Vietnam Petroleum Institute (VPI). One well from the Cuu Long Basin was analysed using six cuttings samples from various stratigraphic levels (Fig. 3). The Nam Con Son Basin was analysed in three wells (NCSa, NCSb, NCSc) covering Oligocene to Miocene stratigraphic intervals (Fig. 4). Three cuttings samples were analysed from well NCSa, five cuttings samples from well NCSb, and two core samples from NCSc. A sample list overview with analysis undertaken can be found in Supplementary Table 1.

Biostratigraphy

Covered thin sections were prepared for calcareous mudstones of 16 cuttings samples of the Nam Con Son Basin (wells NCSa and NCSb) and two cuttings samples of the Cuu Long Basin, and analysed for biostratigraphy, following the approach described in BouDagher-Fadel (2015, 2018a). This primarily uses the Planktonic Zonation scheme (PZ) of BouDagher-Fadel (2018b), which is tied to the biostratigraphical and the radioisotope time scales (as defined by Gradstein et al. 2012 and revised by Cohen et al. 2013).

Heavy mineral separation and analysis

Sample preparation for heavy mineral analyses and zircon enrichment was carried out at Royal Holloway University of London. The friable cuttings and core samples were processed by mortar and pestle, washed and sieved into a 63–250 µm fraction. Heavy minerals were separated using standard heavy liquid lithium heteropolytungstate at a density of 2.89 g/cm^3, using the technique outlined in Mange and Maurer (1992).

Heavy mineral analysis was performed primarily on polished epoxy resin blocks with QEMSCAN by Rocktype with QEMSCAN 10 measurement method that has a resolution of 10 µm. Additional samples from the Cuu Long Basin were analysed with EDS–SEM at the Royal Holloway University of London after the methodology outlined in Hennig-Breitfeld et al. (2019) and Breitfeld et al. (2020a), and Raman spectroscopy (e.g., Andò et al. 2009; Andò and Garzanti, 2014) was conducted on samples from both basins at Chemostrat Ltd. on a Horiba XploRa Raman with a 532 µm laser. Acquired spectra were compared to the RRUFF database (Lafuente et al. 2016) and an internal Chemostrat Ltd. database. Dunkl et al. (2020) demonstrated that electron beam-based methods such as QEMSCAN yield overall results that are comparable to Raman analysis, especially if the heavy mineral assemblage does not contain high proportions of polymorphs (which are not resolvable with electron beam methods) and chain silicates (which are difficult to discriminate with electron beam methods). Supplementary Table 1 displays which method was used for each sample. QEMSCAN results yielded the highest count numbers.

Baryte removal technique

A few cuttings samples contained abundant heavy minerals baryte or anhydrite. Baryte is indicative of drilling mud contamination and anhydrite may also be a drilling additive or be diagenetic. Both minerals can flood and dilute the heavy mineral assemblage and a method to remove the two phases was employed.

Baryte and to a lesser extent anhydrite grains were removed from heavy mineral separates through selective pulverisation using a standard dental amalgamator and acrylic balls. The vibration of the dental amalgamator and the acrylic balls pulverises softer minerals, leaving only more resistant minerals because of the low hardness of baryte and anhydrite (Mohs scale 3 to 3.5) compared to other heavy minerals. This method was adapted and modified from the procedure described by the Arizona Laserchron Center at the University of Arizona (listed as Processing Samples (Min Sep): WIG-L-BUG removal of softer materials) at: https://sites.google.com/laserchron.org/arizonalaserchroncenter/home.

The heavy mineral separates and the acrylic balls of 1/8 mm size were placed into a stainless-steel capsule, which were securely placed onto the dental amalgamator for a short period of time (up to one minute). The vibration of the amalgamator destroyed the targeted soft minerals. The modified heavy mineral separates were rinsed using isopropanol through a 20 µm sieve. The isopropanol and pulverised baryte mixture created a ``milky'' mixture. The remaining hard minerals were washed with a small amount of acetone under a fume hood and subsequently examined under the microscope. If the resulting mixture was not milky or there were still large amounts of baryte visible under the microscope, the process was repeated. Heavy mineral separates were split before employing the method and analysed separately to assess the success of the method, but also to assess the effect on other heavy mineral grains.

LA–ICP–MS zircon geochronology

For zircon concentration the separates were further processed with a Frantz magnetic barrier separator and immersed into di-iodomethane at 3.3 g/cm^3 to maximise the purity of the zircon separates. Zircon grains were imaged in transmitted light to detect cracks or inclusions and cathodoluminescence imaging was performed to identify zoning prior selection of analysis spots for the laser ablation inductively coupled plasma mass spectrometry (LA–ICP–MS).

The methodology used follows the detrital zircon geochronology analysis scheme described in Breitfeld et al. (2020a). U–Pb LA–ICP–MS analysis was performed at Birkbeck College, University of London with a New Wave NWR 193 nm laser ablation system coupled to an Agilent 7700 quadrupole-based plasma ICP–MS with a two-cell sample chamber. A spot size of 25 µm was used for the ablation. The Plešovice zircon standard (337.13 ± 0.37 Ma; Sláma et al. 2008) and a NIST 612 silicate glass bead (Pearce et al. 1997) were used to correct for instrumental mass bias and depth-dependent inter-element fractionation of Pb, Th and U. Data reduction was achieved with the GLITTER software (Griffin et al. 2008). The data were corrected using the common lead correction method of Andersen (2002), which is used as a ^{204}Pb common lead-independent procedure. Supplementary Table 2 displays results of measured Plešovice zircons (weighted mean age: 337.11 ± 0.32 Ma, n = 159, MSWD = 0.08). IsoplotR (Vermeesch 2018) was used for calculation and illustration of zircon standard results (Supplementary Fig. 1).

For grains older than 1000 Ma the age was that obtained from the $^{207}Pb/^{206}Pb$ ratio. For ages younger than 1000 Ma, the ages from the $^{238}U/^{206}Pb$ ratio were used, because ^{207}Pb cannot be measured with sufficient precision, resulting in large analytical errors (Nemchin and Cawood 2005). Concordance was tested using a 10% threshold between the $^{207}Pb/^{206}Pb$ and $^{206}Pb/^{238}U$ ages for ages greater than 1 Ga and between the $^{207}Pb/^{235}U$ and $^{206}Pb/^{238}U$ ages for ages below 1 Ga. Age histograms and probability density plots were created using an R script that adopts the approach of Sircombe (2004) for calculating probability density. A few cores and rims were observed in CL images, and both sites were analysed following the approach by Zimmermann et al. (2018) to detect all age peaks, which is important for provenance studies. Analytical results are presented in Supplementary Table 3 for Cuu Long Basin and Supplementary Table 4 for Nam Con Son Basin. CL images with laser ablation spots of all zircons can be found in Supplementary Fig. 2. For a simple illustration of the detrital zircon data we use a Multi-Dimensional Scaling (MDS) plot for detrital zircon age distributions (Vermeesch 2013). The MDS plot is based on a dissimilarity matrix between pairwise samples, using here the two-sample Kuiper distance test, and generated with the R provenance package by Vermeesch et al. (2016).

Results

Biostratigraphy

The Cuu Long Basin samples are dominated by clastic sediments with strong fluvial or deltaic influence and only very rare non-age diagnostic foraminifera were observed. Samples from the Nam Con Son Basin yielded foraminifera which enable high resolution biostratigraphy for the Dua Formation (T30) and the Thong Formation (T40&50). The lowermost analysed succession, the Cau Formation, did not yield age-diagnostic foraminifera. The Dua Formation is dated as Early Miocene with the lower part having a foraminifera assemblage belonging to the Planktonic Foraminiferal zones N5 to N6 (presence of *Catapsydrax stainforthii* and *Catapsydrax dissimilis*) with an age of 21.0 to 17.2 Ma. Fragments of upper Oligocene to lower Miocene reefal larger benthic foraminifera (*Lepidocyclina* sp.) are reworked into this inner neritic foraminiferal assemblage. The uppermost sample (NCSa-2) belongs to zone N7 (based on the presence of *Globorotalia miozea* and *Globigerina connecta*) with an age of 17.2 to 17.0 Ma (Table 1). The overlying Thong Formation samples yielded a Langhian foraminifera assemblage diagnostic for Planktonic Foraminiferal zone N8b–N9a (presence of *Praeorbulina glomerosa*) with an age of 15.4 to 14.5 Ma (Table 1). This suggests a short hiatus between the two formations as zone N8a was not observed. Relative stratigraphic position of Nam Con Son Basin samples with age diagnostic foraminifera is displayed in Fig. 4. Assorted and index foraminifera photomicrographs from the Nam Con Son Basin samples are displayed in Fig. 5.

U–(Th)–Pb zircon geochronology

All of the samples analysed yielded zircons significantly older than the depositional ages, and therefore, no age estimate for the formations can be made from the detrital zircons.

Cuu Long Basin

Tra Tan Formation (D)

Sample CLB9.1 from the lower part of the Tra Tan Formation was analysed and 128 concordant U–Pb zircon ages were acquired from 134 zircons. CL imagery revealed predominantly oscillatory zoned or sector zoned euhedral zircons. No obvious core–rim structures were observed. A single grain had a core of 272 ± 5 Ma and with a slightly younger age of 257 ± 6 Ma from edge of the grain. The sample is dominated by Cretaceous zircons, which form about 87% (111 out of 128) of the zircon assemblage (Fig. 6). Cretaceous ages range from c. 70 to 122 Ma with a dominant narrow peak between 90 and 100 Ma. There are 16 ages that scatter from the Early Jurassic to the Devonian, with a small Permian population (11 ages). The oldest grain is 1758 ± 22 Ma and the youngest is 70 ± 1 Ma.

Lower Bach Ho Formation (BI.1)

Sample CLB6.1 from the Lower Bach Ho Formation was analysed and 135 detrital zircon grains yielded 131 concordant ages. Zircons are generally oscillatory zoned, and no core–rim structures were observed. The sample

Table 1 Biostratigraphy results of the Cuu Long and Nam Con Son basins. Samples from well NCSa yielded a number of age diagnostic foraminifera. Age based on first appearance Planktonic Foraminiferal zones after BouDagher-Fadel (2015, 2018b) relative to the biostratigraphical time scale (as defined by Gradstein et al. 2012)

Samples	Seismic sequence	Formation	Microfacies	Components (those in green are caved, while those in red are reworked)	Depositional environment	Age
Nam Con Son Basin						
NCSb-3	T40/T50	Thong	Micritic wackestone of extremely rare foraminifera	*Neogloboquadrina dutertrei, Orbulina universa, Truncorotalia tosaensis, Bulimina* sp., *Catapsydrax* sp., *Praeorbulina glomerosa, Globoquadrina dehiscens, Dentoglobigerina altispira, Globigerina* sp., *Catapsydrax parvulus*	Shallow inner neritic	Langhian, N8b—N9a, 15.4–14.5 Ma
NCSb-4	T40/T50	Thong	Micritic wackestone of extremely rare foraminifera	*Globigerina* sp.	Shallow inner neritic	Cenozoic
NCSb-5	T40/T50	Thong	Micritic wackestone of extremely rare foraminifera	*Globulina* sp., *Globigerina* sp.	Shallow inner neritic	Cenozoic
NCSb-8	T30	Dua	Micritic wackestone of extremely rare foraminifera	*Globigerina* spp.	Shallow inner neritic	Cenozoic
NCSb-9	T30	Dua	Micritic wackestone of extremely rare foraminifera	*Globigerina* spp.	Shallow inner neritic	Cenozoic
NCSb-10	T30	Dua	Micritic wackestone of extremely rare foraminifera	*Globigerina* spp.	Shallow inner neritic	Cenozoic
NCSb-12	T30	Dua	Micritic wackestone of extremely rare foraminifera	*Globigerina* spp.	Shallow inner neritic	Cenozoic
NCSb-18	T30	Dua	Micritic wackestone of extremely rare foraminifera	Recrystallised algae, *Globigerina* sp.	Shallow inner neritic	Cenozoic
NCSb-21	T20	Cau	Micritic wackestone of extremely rare foraminifera	*Orbulina suturalis*	Inner to outer neritic	Cenozoic
NCSa-1	T40/T50	Thong	Micritic wackestone of planktonic foraminifera	*Candeina nitida, Orbulina suturalis, Neogloboquadrina acostaensis, Globigerina decoraperta, Globoquadrina dehiscens, Dentoglobigerina altispira, Praeobitolina transitoria, Praeorbulina glomerosa, Paragloborotalia mayeri*	Inner to outer neritic	Langhian, N8b—N9a, 15.4–14.5 Ma
NCSa-2	T30	Dua	Micritic wackestone of planktonic foraminifera	*Globorotalia scitula, Orbulina suturalis, Neogloboquadrina* sp., *Candeina nitida, Orbulina universa, Globorotalia miozea, Globigerina connecta, Paragloborotalia mayeri*	Inner to outer neritic	Late Burdigalian, N7, 17.2–17.0 Ma
NCSa-3	T30	Dua	Micritic wackestone of extremely rare foraminifera	*Globigerina* sp.	Shallow inner neritic	Cenozoic

Table 1 (continued)

Samples	Seismic sequence	Formation	Microfacies	Components (those in green are caved, while those in red are reworked)	Depositional environment	Age
NCSa-4	T30	Dua	Micritic wackestone of extremely rare foraminifera with Eocene reworking	*Globigerina praebulloides, Globigerina venezuelana, Catapsydrax stainforthi, Globigerinatheka barri, Subbotina* sp.	Inner neritic	Early Miocene, N5-N6, 21.0–17.2 Ma
NCSa-5	T30	Dua	Micritic wackestone of extremely rare foraminifera	*Globigerina spp., Globigerinoides spp., Catapsydrax dissimilis, Globigerinoides quadrilobatus*	Inner neritic	Early Miocene, N5-N6, because of underlying sample
NCSa-6	T30	Dua	Micritic wackestone of extremely rare foraminifera	*Catapsydrax stainforthi, Paragloborotalia mayeri, Catapsydrax dissimilis, Globigerina* sp., fragment of *Lepidocyclina* sp.,	Shallow inner neritic	Early Miocene, N5-N6, 21.0–17.2 Ma
NCSa-7	T20	Cau	Micritic wackestone of extremely rare foraminifera	*Globigerina* sp.	Shallow inner neritic	Cenozoic
Cuu Long Basin						
CLB2.3	BII	Con Son	Micritic wackestone of extremely rare recrystallised foraminifera	*Rotalia* sp., echinoid spp.	shallow marine environment	Cenozoic
CLB5	BI.1	Lower Bach Ho	Micritic cuttings	small rotaliid spp.	Indet	Indet

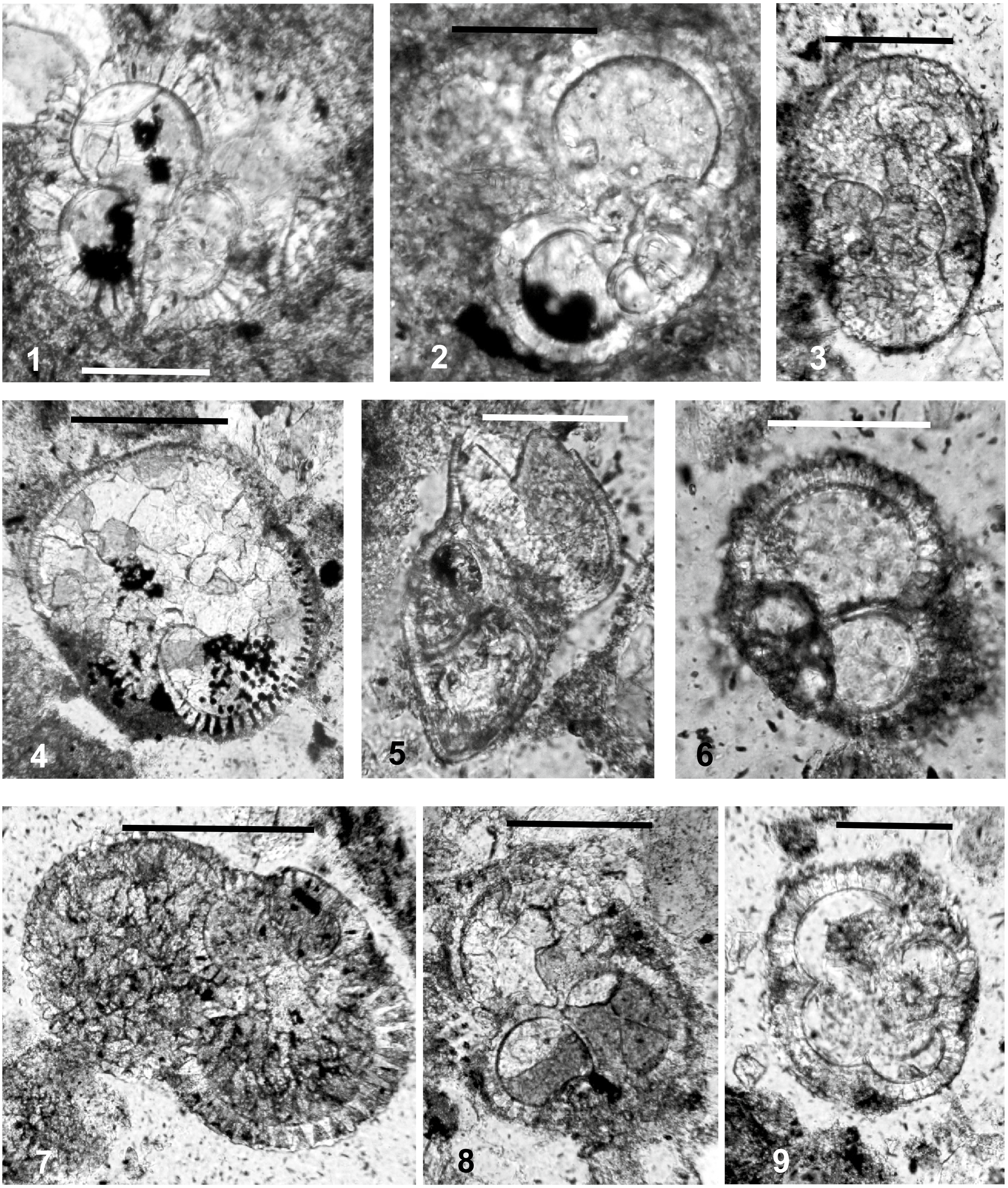

Fig. 5 Plate of representative foraminifera of the Nam Con Son samples. 1—*Praeorbulina glomerosa* (Blow), NCSb-3. Thong Formation. 2—*Catapsydrax dissimilis* (Cushman and Bermudez), NCSb-3. Thong Formation. 3—*Praeorbulina transitoria* (Blow), NCSa-1. Thong Formation. 4—*Dentoglobigerina altispira* (Cushman and Jarvis), NCSa-1. Thong Formation. 5—*Globorotalia miozea* Finlay, NCSa-2. Dua Formation. 6—*Globigerina connecta Jenkins,* NCSa-2. Dua Formation. 7—*Globorotalia mayeri* Cushman and Elisor, NCSa-2. Dua Formation. 8—*Globigerina praebulloides* Blow, NCSa-4. Dua Formation. 9—*Catapsydrax stainforthi* Blow, Loeblich and Tappan, NCSa-6. Dua Formation. Scale bars on photomicrographs 1 – 9 = 0.2 mm

is dominated by Cretaceous zircons which form about c. 82% (107 out of 131) of the assemblage (Fig. 6). The Cretaceous ages range from c. 75 to 116 Ma similar to CLB9.1 with a dominant peak between 80 and 100 Ma. The only other Phanerozoic age population is 23 Permian–Triassic ages. There are two Precambrian ages, one each in the Neoproterozoic and Paleoproterozoic. The oldest age is 1856 ± 19 Ma (Paleoproterozoic) and the youngest grain is 74.6 ± 0.8 Ma (Cretaceous).

Upper Bach Ho Formation (BI.2)

Sample CLB4.1 from the Upper Bach Ho Formation was analysed and 124 concordant ages were acquired from 128 zircon grains. Zircons show oscillatory zoned internal structures. Like the underlying Lower Bach Ho samples, the Upper Bach Ho zircons are predominantly Cretaceous which form about 84% (104 out of 124) of the assemblage (Fig. 6). The Cretaceous zircon ages range from c. 74 to 145 Ma with a major peak between 90 to 110 Ma, and there are significant populations between 80 to 90 and around c. 125 Ma. The analysed sample contains two Jurassic zircons and 17 Permian–Triassic zircons. The sample has only a single grain older than Permian at 2538 ± 9 Ma. The youngest age is 73.8 ± 1 Ma.

Con Son Formation (BII)

Samples CLB2.1 and CLB2.3 from the Con Son Formation were analysed. The two samples have similar zircon age populations and are displayed together as CLB2_1–3. 188 concordant ages were acquired from 193 zircon grains. Zircon grains are predominantly sector zoned or show oscillatory zoning. In contrast to the underlying samples, a number of rounded dark zircons were observed. A single Neoproterozoic grain showed core–rim structures with a core of 914 ± 11 Ma and a rim of 636 ± 8 Ma. No other core–rim structures were observed. 188 concordant ages were acquired from 193 zircon grains. In contrast to the underlying formations that are almost entirely composed of Cretaceous zircons, the Con Son samples are dominated by Triassic zircons and other heterogeneous age populations (Fig. 6). 32% (60 out of 188) ages are Triassic with the majority being between 220 to 230 Ma and a small Permian tail that goes up to c. 280 Ma. The second most prominent age population is Cretaceous with c. 14% of ages (26 out of 188). The Cretaceous population ranges from c. 80 to 140 Ma, and most ages are between c. 90 and 120 Ma. Other Phanerozoic age populations are Jurassic and other ages scattered throughout the Palaeozoic of which Silurian–Ordovician ages are the most common. 52 ages are Precambrian and there are populations at c. 700–800 Ma, 1.2 Ga, between 1.8 and 1.9 Ga, which forms the most significant population, and at c. 2.5 Ga. There are three zircon ages at c. 2.8 Ga with the oldest being 2764 ± 8 Ma. The youngest zircon was found in sample CLB2.1 and is 78 ± 2 Ma.

Dong Nai Formation (BIII)

Sample CLB1.1 from the Dong Nai Formation yielded 129 concordant ages from 132 detrital zircons. CL imagery revealed predominantly patchy, zoned or sector zoned zircons. An abundance of subrounded grains with dark CL was observed. Core–rim structures are very rare, and the one observed core yielded an age of 621 ± 7 Ma with a rim of 214 ± 2 Ma. The sample is dominated by Upper Triassic zircons with a long tail of ages that range into the Late Carboniferous (Fig. 6). Triassic ages form c. 34% (44 out of 129) of the whole assemblage, with 26% of the whole assemblage being Late Triassic. Other zircon populations are Cretaceous with a Late Cretaceous peak between 90 and 100 Ma, Ordovician–Silurian, and Precambrian. Those Precambrian zircons are dominated by a strong age peak between 1.8 and 1.9 Ga (Fig. 6). The only other significant Precambrian age population lies between 700 and 800 Ma. The oldest analysed zircon is 3541 ± 5 Ma. The youngest three zircons are Oligocene to Eocene in age and range from 35.1 to 50 Ma, but do not overlap in error and are significantly older than the depositional age. Similar young zircons were not observed in the other Cuu Long Basin samples.

Nam Con Son Basin

Cau Formation (T20)

The Cau Formation was analysed in three samples from cuttings (NCSa-7, NCSb-19, NCSb-23) and two samples from core (NCSc-1, NCSc-2). The combined age plot for the five samples is displayed in Fig. 7 as NCS-3. The three cuttings samples yielded only a very small number of zircons. In total 300 concordant ages were acquired from 310 zircons. Zircon shapes range from euhedral to rounded with the latter being more abundant. Euhedral grains often show rounded edges and are frequently oscillatory zoned, while rounded grains appear often dark grey or patchy zoned in CL. Core–rim structures were occasionally observed. The Cau Formation contains predominantly Phanerozoic zircons (64%) with a major peak in the Triassic that extends into the Permian. Cretaceous zircons form the second-most abundant Phanerozoic population. There are Jurassic, Silurian–Ordovician and Cambrian zircon

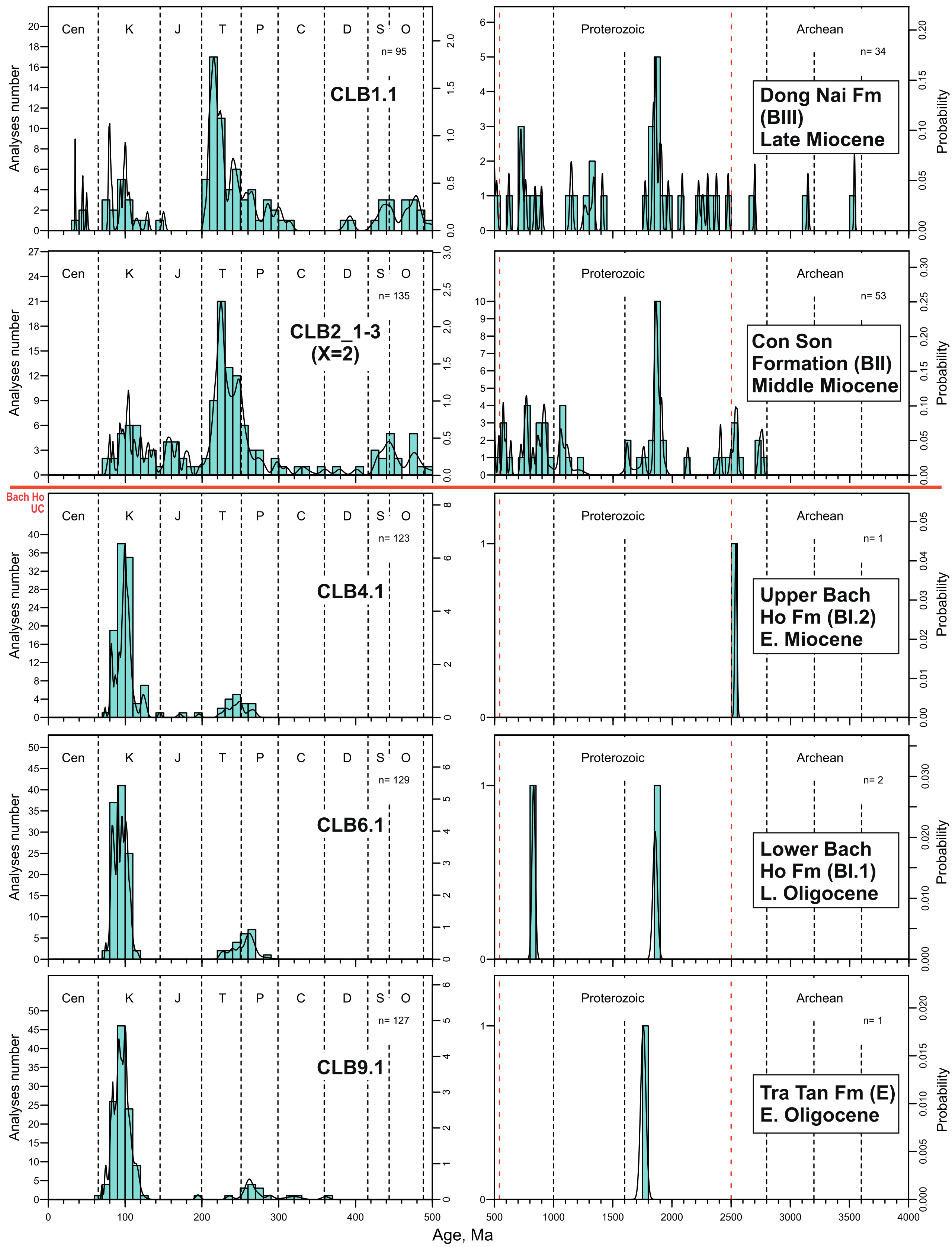

CLB1.1
n= 95
n= 34
Dong Nai Fm (BIII) Late Miocene
CLB2_1-3 (X=2)
n= 135
n= 53
Con Son Formation (BII) Middle Miocene
Bach Ho UC
CLB4.1
n= 123
n= 1
Upper Bach Ho Fm (BI.2) E. Miocene
CLB6.1
n= 129
n= 2
Lower Bach Ho Fm (BI.1) L. Oligocene
CLB9.1
n= 127
n= 1
Tra Tan Fm (E) E. Oligocene
Cen
K
J
T
P
C
D
S
O
Proterozoic
Archean
Analyses number
Probability
Age, Ma

◂**Fig. 6** Detrital zircon age histograms with probability density curves for the Cuu Long Basin samples in stratigraphic order. Samples from the Tra Tan (horizon D) and Bach Ho (horizons BI.1 and BI.2) are dominated by Cretaceous zircons. Unconformably on top are the Con Son (horizon BII) and Dong Nai (horizon BIII) formations, which display a heterogeneous detrital zircon age spectrum, dominated by Triassic ages. The Bach Ho Unconformity at c. 16 to 20.5 Ma marks the major provenance boundary. Bin size of 10 Ma for Phanerozoic ages and 50 Ma for Precambrian ages. X = number of samples

populations. The Precambrian zircons are dominated by Paleoproterozoic ages of 1.75 to 1.95 Ga which make up c. 10.6% of the total age distribution. Scattered ages between c. 700 Ma and 1.2 Ga and a narrow Archean peak at c. 2.5 Ga are other Precambrian populations. The oldest age of 2874 ± 9 Ma was from NCSc-1, and the youngest zircon was 72.9 ± 1 Ma from NCSc-2.

Dua Formation (T30)

The Dua Formation was analysed in samples NCSa-4, NCSb-10, and NCSb-13. All three samples show very similar detrital zircon age populations and are displayed together as NCS-2. 398 concordant ages were acquired from 403 zircon grains. Zircon grains are relatively similar to the Cau Formation in being dominated by dark grey CL rounded to sub-rounded varieties. The Dua Formation has two main zircon age populations, a Permo-Triassic population that forms a double peak in the Late Permian and early Late Triassic and an older Paleoproterozoic age population around c. 1.8 to 1.9 Ga (Fig. 7). There are almost equal numbers of Phanerozoic (206) and Precambrian (192) zircons. Besides the Permo-Triassic age peak, other Phanerozoic grains are Cretaceous, Upper Jurassic and Ordovician–Silurian with some scattered ages between. The Precambrian has a very wide age population of c. 600 to 1150 Ma, a dominant peak at 1.8–1.9 Ga and a small peak at c. 2.5 Ga. The oldest age was 3693 ± 6 Ma in NCSa-4, and the youngest zircon was 41.9 ± 0.5 Ma in NCSb-10.

Thong Formation (T40&50)

The Thong Formation was analysed in samples NCSa-1 and NCSb-1. Both samples show very similar zircon age populations and are displayed together as NCS-1. 164 concordant ages were acquired from 169 zircon grains. Zircons show predominantly homogenous or oscillatory zoning in CL imagery for euhedral grains, and dark CL for subrounded to rounded grains that dominate the assemblage. Dark areas were usually associated with Precambrian ages. Like the underlying Dua Formation, the Thong Formation is dominated by Triassic zircon ages with a significant number of Precambrian zircons (Fig. 7). In contrast to the Dua Formation, the number of Permian and Cretaceous zircons is lower. The Triassic zircon population forms about 24% (40 out of 164) of the assemblage. The only other significant Phanerozoic age populations are Permian (c. 5%) and Ordovician–Silurian (c. 7%). Only c. 3% of zircons are Cretaceous, and there are small numbers of Jurassic and Carboniferous grains. The number of Precambrian zircons (76) is almost as high as the number of Phanerozoic zircons (88). The Precambrian zircon ages form peaks at c. 900–1000 Ma, c. 1.7–1.9 Ga, and c. 2.5 Ga with scattered ages between. In contrast to the underlying formations, 750 Ma to 1.2 Ga zircons form the dominant Precambrian zircon age assemblage. The oldest age was 2785 ± 12 Ma in NCSb-1, and the youngest zircon was 44.8 ± 0.6 Ma (also in NCSb-1).

Heavy mineral analysis

Heavy mineral results in this study were acquired using three different methods, which in general yielded very comparable results. EDS–SEM and QEMSCAN are electron beam methods which cannot differentiate between TiO_2 polymorphs, whereas Raman spectroscopic analysis can differentiate between rutile, brookite and anatase. Raman results generally indicated slightly more total TiO_2 polymorphs than the electron beam methods, which is likely a function of composite anatase grains that are below the threshold for identification by the electron beam methods, but still result in a strong anatase Raman shift signal. The proportion of TiO_2 polymorphs is likely, therefore, slightly overestimated in the samples analysed by Raman spectroscopy compared to the EDS or QEMSCAN results. Nevertheless, results are consistent. For simplification, in this paper the three polymorphs rutile, brookite and anatase are listed as rutile. Other polymorphs (such as aluminosilicates) were not found. Baryte was discarded from the heavy mineral assemblage, because it was used as a drilling additive. Opaque minerals were also analysed, but due to identification uncertainties using different methods as well as a possible diagenetic origin (e.g., pyrite) no provenance interpretation is given. Heavy mineral proportions are listed in Table 2 and count numbers are listed in Supplementary Table 5.

Cuu Long Basin

The heavy mineral assemblage of the Tran Tra Formation (D) sample CLB9.1 consists of abundant translucent heavy minerals which make about 87% of the total assemblage. Opaque minerals are subordinate, with pyrite (12.5% of the total heavy mineral assemblage) being the most abundant. The translucent heavy mineral assemblage is dominated by apatite (39.7%), rutile (26%) and zircon (22.7%) (Fig. 8A). The heavy mineral assemblage of the overlying Lower Bach Ho Formation sample (BI.1) CLB6.1 is also dominated by translucent heavy minerals which make c. 92% of the

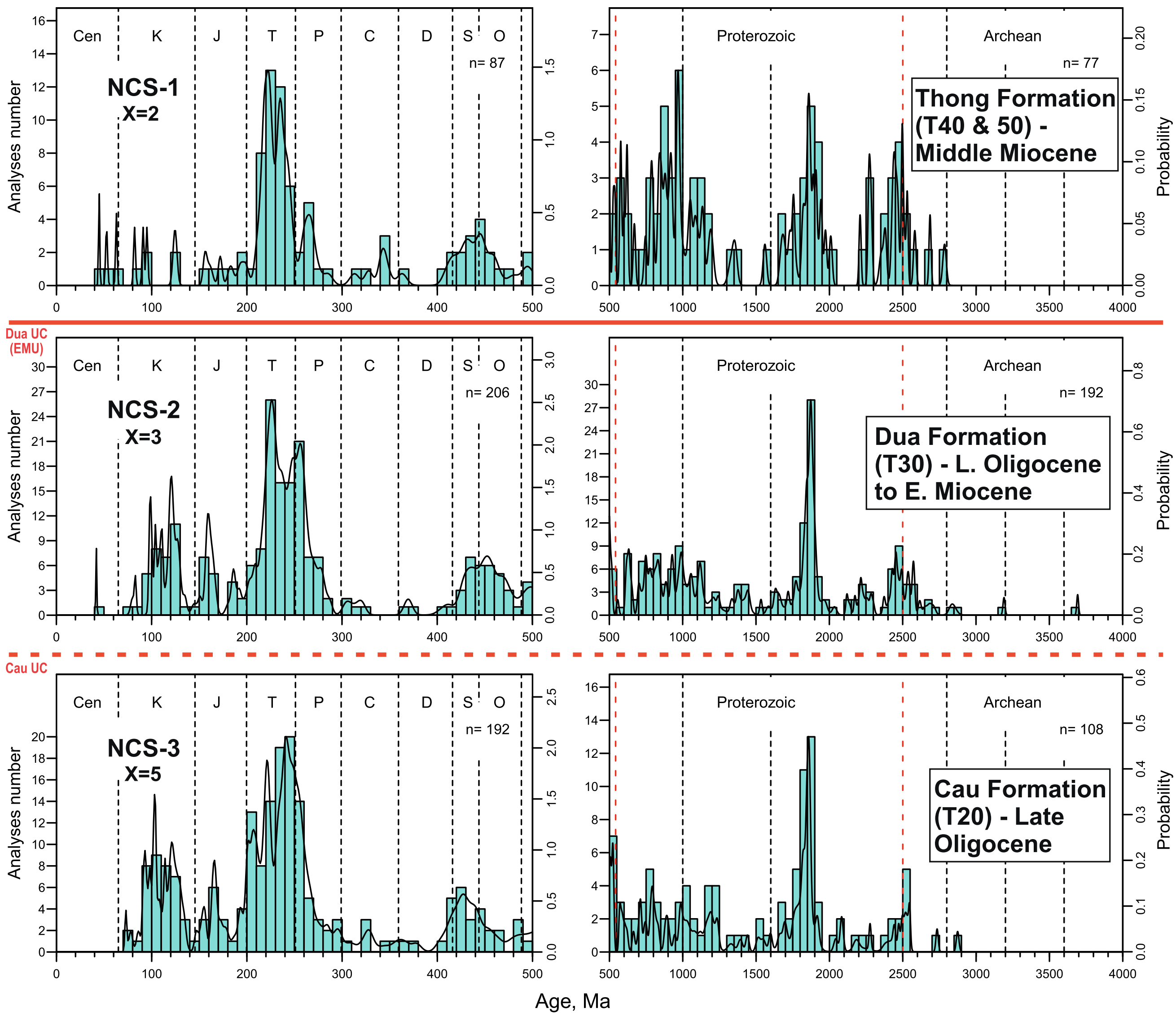

Fig. 7 Detrital zircon age histograms with probability density curves for the Nam Con Son Basin samples in stratigraphic order. Samples from the respective formations have been combined (X = number of samples). The Cau and Dua Formation samples display a heterogeneous zircon age distribution with characteristic peaks in the Permian–Triassic, Cretaceous, Ordovician–Silurian and Paleoproterozoic (c. 1.8 Ga). The Dua Formation has thereby significant more Precambrian ages as the Cau Formation, which may be related to unroofing of a source area. The Cau Unconformity separates the two formations. The Thong Formation above the Dua Formation shows an increase in 800 to 1000 Ma and c. 2.5 Ga zircons, typically for Sibumasu, suggesting a new river system supplying material. The Dua Unconformity marks the boundary at c. 15.4 to 17 Ma. Bin size of 10 Ma for Phanerozoic ages and 50 Ma for Precambrian ages. Supplementary Figure 3 displays the histograms for the individual NCSB samples

total heavy mineral assemblage. Opaque minerals (pyrite, ilmenite) are subordinate. The translucent heavy mineral assemblage (Fig. 8A) is dominated by epidote (43.5%), zircon (17.1%), rutile (13.6%), garnet (5.7%) and tourmaline (5.4%) with minor apatite (3%), titanite (1.8%), sphalerite, monazite and Cr-spinel (all traces only). The Upper Bach Ho Formation sample (BI.2) CLB4.1 has a very similar heavy mineral assemblage to the Lower Bach Ho Formation. Translucent heavy minerals form c. 61.5% of the assemblage with opaque minerals consisting of pyrite (67.9%), hematite (30.5%) and traces of ilmenite. Translucent heavy minerals are dominated by epidote (57.1%), rutile (17.6%), tourmaline (8.6%), apatite (7.1%), zircon (3.3%) and garnet (2.9%) (Fig. 8A). Fluorite, monazite, sphalerite and topaz are present in traces.

The Con Son Formation (BII) heavy mineral samples CLB2.1, CLB2.3 and the Dong Nai Formation (BIII) sample CLB1.1 show very similar heavy mineral proportions and record a major change from the underlying Bach Ho Formation. In contrast to the underlying two formations the heavy

Table 2 Heavy mineral proportions of the analysed CLB and NCSB samples. Mineral ratios after Morton and Hallsworth (1994), Morton (2007), and ZTR (zircon–tourmaline–rutile) index after Hubert (1962)

Sample ID	Formation	Seismic Group	Rutile (TiO_2)	Cr-spinel	Monazite	Xenotime	Sphalerite	Zircon	Tourmaline	Garnet	Epidote	Titanite	Staurolite	Amphibole	Pyroxene	Apatite	Topaz	HM total	Opaque total	Translucent -%	Opaque -%	ZTR	RZi	GZi	ATi	MZi	CZi	ZTi
Cuu Long Basin																												
CLB1.1	Dong Nai	BIII	38.9	1.1	1.7	0.0	0.0	4.4	18.3	16.1	1.7	0.6	0.6	0.0	0.6	16.1	0.0	180	268	40.2	59.8	61.7	89.7	78.4	46.8	27.3	20.0	19.5
CLB2.1	Con Son	BII	38.6	0.9	3.3	0.1	0.7	3.0	15.8	11.7	0.1	0.0	0.1	2.3	2.4	21.1	0.0	888	1168	43.2	56.8	57.4	92.7	79.4	57.2	51.8	22.9	16.2
CLB2.3	Con Son	BII	48.6	1.4	0.0	0.0	0.0	5.6	15.3	12.5	2.8	0.0	0.0	0.0	4.2	9.7	0.0	72	61	54.1	45.9	69.4	89.7	69.2	38.9	0.0	20.0	26.7
CLB4.1	U. Bach Ho	BI.2	17.7	0.0	0.5	0.0	1.4	3.3	8.6	2.9	57.4	0.0	0.0	0.0	0.0	7.2	1.0	209	131	61.5	38.5	29.7	84.1	46.2	45.5	12.5	0.0	28.0
CLB6.1	L. Bach Ho	BI.1	15.0	0.1	0.2	0.0	0.5	18.8	6.0	6.3	47.9	2.0	0.0	0.0	0.0	3.3	0.0	5329	471	91.9	8.1	39.8	44.4	25.1	35.4	1.2	0.4	75.9
CLB9.1	Tra Tran	D	26.0	0.1	0.4	0.1	1.8	22.7	7.5	1.2	0.1	0.3	0.0	0.1	0.0	39.7	0.0	938	142	86.9	13.1	56.2	53.4	4.9	84.2	1.8	0.5	75.3
Nam Con Son Basin																												
NCSb-1	Thong	T40&T50	47.8	0.9	2.6	0.0	5.2	4.3	9.9	1.7	0.4	0.4	0.0	0.0	0.0	26.7	0.0	232	2088	10.0	90.0	62.1	91.7	28.6	72.9	37.5	16.7	30.3
NCSa-1	Thong	T40&T50	43.2	1.1	1.1	0.0	0.0	12.1	20.1	5.1	0.4	0.7	0.0	0.0	0.0	16.1	0.0	273	665	29.1	70.9	75.5	78.1	29.8	44.4	8.3	8.3	37.5
NCSa-4	Dua	T30	75.6	0.8	0.8	0.0	0.0	5.7	8.9	4.9	0.0	0.0	0.0	0.0	0.0	3.3	0.0	123	17	87.9	12.1	90.2	93.0	46.2	26.7	12.5	12.5	38.9
NCSb-10	Dua	T30	83.3	0.0	0.0	0.0	0.0	12.1	3.0	0.0	0.0	1.5	0.0	0.0	0.0	0.0	0.0	66	3	95.7	4.3	98.5	87.3	0.0	0.0	0.0	0.0	80.0
NCSb-13	Dua	T30	66.8	1.7	1.3	0.5	0.7	16.4	4.0	3.0	0.1	0.0	0.0	0.1	0.0	5.5	0.0	844	93	90.1	9.9	87.2	80.3	15.3	57.5	7.4	9.2	80.2
NCSa-7	Cau	T20	48.4	3.2	4.8	0.0	0.0	17.7	9.7	9.7	0.0	0.0	0.0	0.0	0.0	6.5	0.0	62	123	33.5	66.5	75.8	73.2	35.3	40.0	21.4	15.4	64.7
NCSc-1	Cau	T20	70.6	0.0	1.5	0.0	0.0	8.8	7.4	2.9	0.0	0.0	0.0	0.0	0.0	8.8	0.0	68	333	17.0	83.0	86.8	88.9	25.0	54.5	14.3	0.0	54.5
NCSb-19	Cau	T20	64.5	0.3	6.4	0.0	2.0	13.7	4.4	0.0	0.0	0.0	0.0	0.0	0.0	8.7	0.0	344	606	36.2	63.8	82.6	82.5	0.0	66.7	31.9	2.1	75.8
combined Nam Con Son samples																												
NCS-1	Thong	T40&50	45.3	1.0	1.8	0.0	2.4	8.5	15.4	3.6	0.4	0.6	0.0	0.0	0.0	21.0	0.0	505	2753	15.5	84.5	69.3	84.2	29.5	57.6	17.3	10.4	35.5
NCS-2	Dua	T30	68.9	1.5	1.2	0.4	0.6	14.8	4.5	3.0	0.2	0.0	0.0	0.1	0.0	4.8	0.0	1033	113	90.1	9.9	88.3	82.3	16.8	51.5	7.3	8.9	76.5
NCS-3	Cau	T20	63.3	0.6	5.5	0.0	1.5	13.5	5.5	1.7	0.0	0.0	0.0	0.0	0.0	8.4	0.0	474	1062	30.9	69.1	82.3	82.4	11.1	60.6	28.9	4.5	71.1

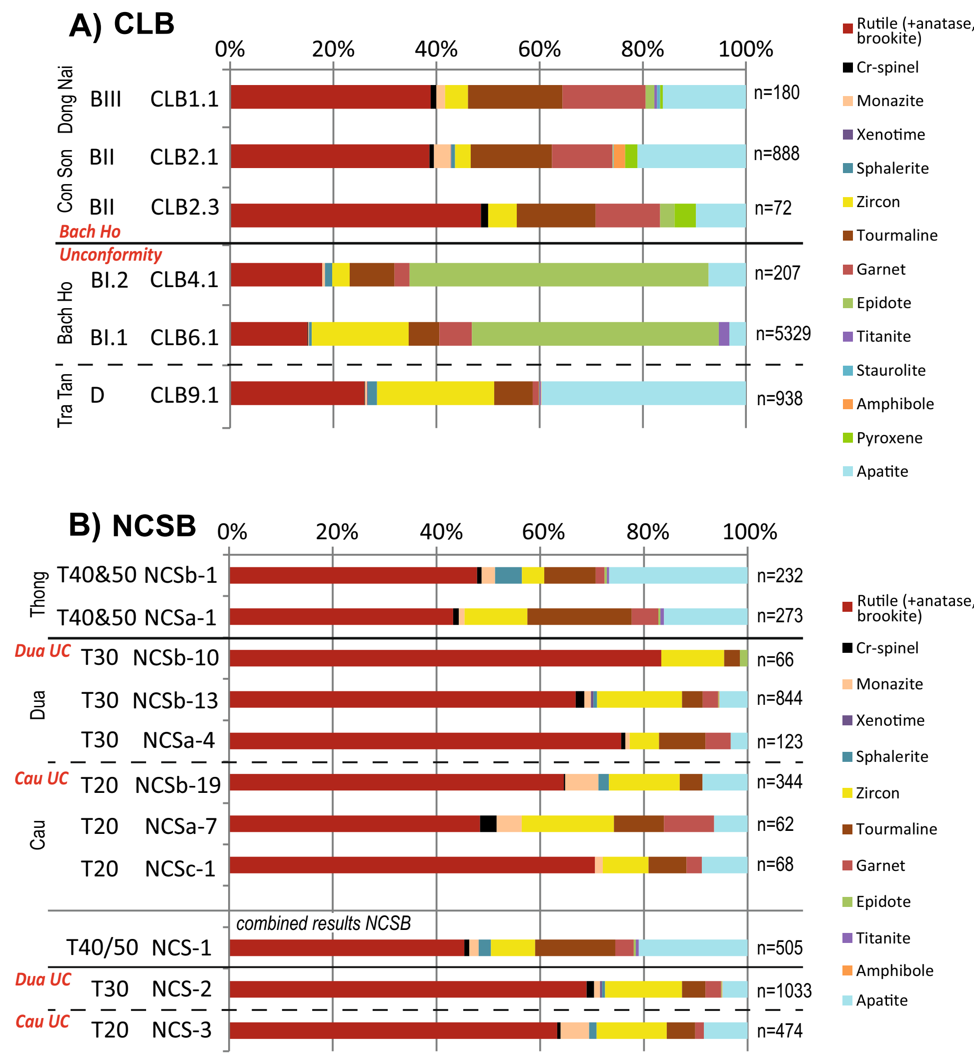

Fig. 8 Heavy mineral assemblages of the studied intervals. **A**) Cuu Long Basin samples: The Tra Tan and Bach Ho Formation samples (D to BI.2) are dominated by unstable varieties, with D dominated by apatite and BI by epidote. The Bach Ho Unconformity marks a major change in heavy mineral assemblages. The overlying Con Son and Dong Nai formations (BII to BIII) are dominated by rutile, tourmaline, garnet and zircon. **B**) Nam Con Son Basin samples displayed per samples (upper panel) and per formation/seismic sequence (lower panel). T20 (Cau) and T30 (Dua) are dominated by ultra-stable heavy minerals, especially rutile. The overlying T40&T50 (Thong) has characteristic higher apatite proportions

mineral assemblages are dominated by opaque minerals. Pyrite makes up to 50% of the total heavy mineral assemblage and hematite (up to 21%) and ilmenite (up to c. 7%). Translucent heavy minerals form only around 40 to 54% of the total heavy mineral assemblage with rutile (up to 48.6%), apatite (9.7 to 21.1%), tourmaline (15.3 to 18.3%) and garnet (11.7 to 16.1%) being the most abundant (Fig. 8A). Zircon (up to 5.6%), monazite (up to 3.3%), pyroxene (up to 4.2%), epidote (up to 2.8%), amphibole (up to 2.3%) and Cr-spinel (up to 1.4%) are subordinate (Fig. 8A). Traces of xenotime, sphalerite, titanite and staurolite were also observed.

The Tra Tan Formation and the Bach Ho Formation samples show some similarities in relevant heavy mineral indices, despite the high amount of epidote in the Bach Ho Formation. The ZTi and CZi values and the moderate RZi are similar in the lower Bach Ho Formation and the Tra Tan Formation samples (Fig. 9A). The two samples differ in ZTR which decreases sharply in the Lower Bach Ho Formation as a result of abundant epidote, in GZi which increases as garnet increases and in ATi which decreases sharply as apatite decrease (Fig. 9A), thus indicating some source differences for the two formations. The Upper Bach Ho Formation sample (CLB4.1), despite its very similar heavy mineral proportions to the Lower Bach Ho sample (CLB6.1), has indices that indicate a change within the formation. Like the Lower Bach Ho Formation ZTR is low, ATi is moderate, and CZi is 0 (Fig. 9A). In contrast, GZi and RZi increase significantly and ZTi decreases, which is more similar to the overlying formations (Fig. 9A). Up section the heavy mineral indices show a major change between the Bach Ho Formation and the overlying Con Son and Dong Nai Formations. The ZTR values of the Con Son and Dong Nai Formation increases slightly from the underlying Bach Ho Formation as a result of the higher abundance of rutile and tourmaline (Fig. 9A). There is also an increase in RZi (up to 93) and a decrease of ZTi (down to 16) in the Upper Bach Ho Formation (Fig. 9A). In addition, there is a sharp increase in CZi (Fig. 9A), all supporting a significant source change at the base of the Con Son Formation, which may have started within

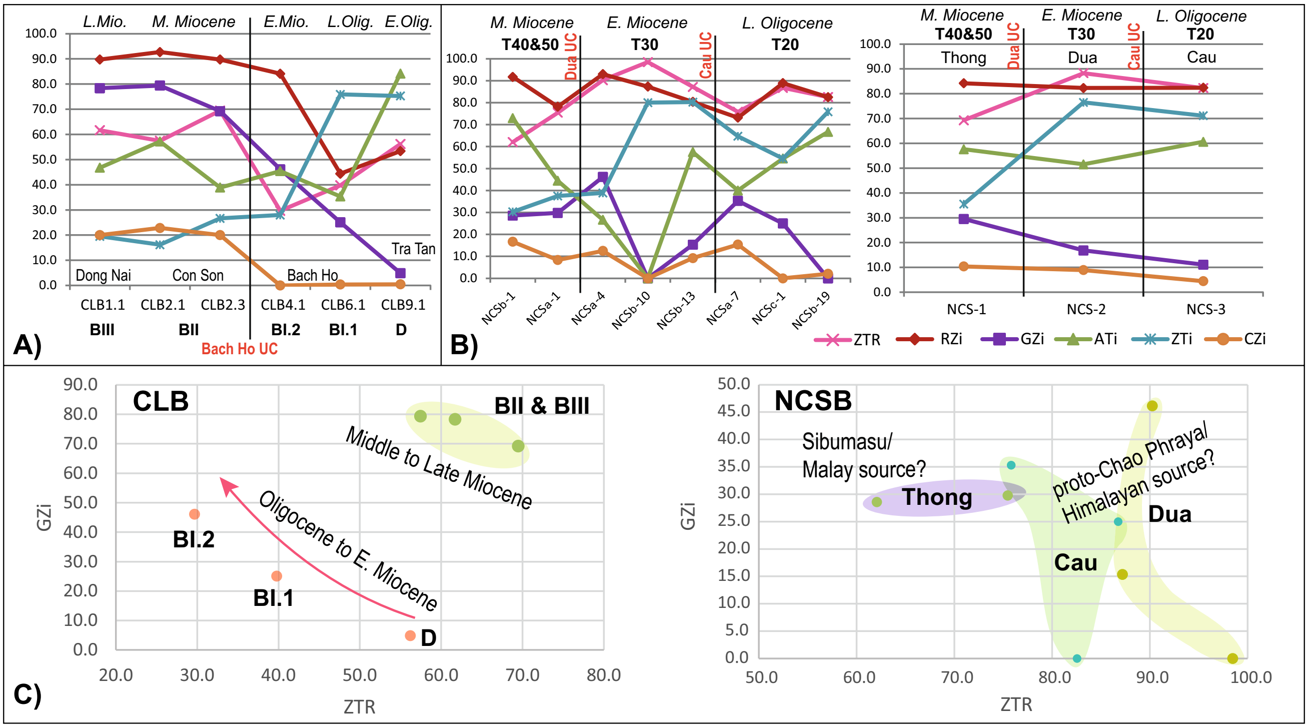

Fig. 9 Heavy mineral indices plots, using the ZTR (Hubert 1962), RZi, GZi, ATi, ZTi and CZi (Morton and Hallsworth 1994; Morton 2007). **A**) CLB heavy mineral data shows a significant change at the Bach Ho Unconformity between the underlying Bach Ho Formation and the overlying Con Son. Indices ZTR, CZi, GZi and RZi best illustrate the change in provenance, while other indices are more variable. **B**) NCSB heavy mineral data is displayed per sample (left panel) and per seismic sequence/formation (right panel). Indices are very similar, only the ZTR, ZTi and GZi show some variation from T20/30 to T40&50. **C**) ZTR-GZi biplots for the CLB and NCSB can be used to distinguish between the different formations. CLB data clearly separates into the Tra Tan-Bach Ho trend (red) and into the Con Son-Dong Nai (green). The three formation of the NCSB are also separated by the bi-plot with the Cau and Dua formations being very similar, and the Thong Formation having a slightly different heavy mineral assemblage

the Upper Bach Ho Formation. The Dong Nai Formation shows a relatively similar heavy mineral assemblage with similar heavy mineral indices to the underlying Con Son Formation (Fig. 9A), suggesting no major source changes for the two formations. The ZTR-GZi bi-plot best displays the two different main assemblages observed in the CLB samples (Fig. 9C).

Nam Con Son Basin

Samples NCSa-7, NCSb-19 and NCSc-1 from the Cau Formation (T20) were analysed for heavy minerals. The heavy mineral assemblage is dominated by opaque minerals with up to 83% of the total heavy mineral assemblage; pyrite is the most abundant. Translucent heavy minerals form c. 17 to 36% of the total assemblage and are dominated by rutile (48.4% to 70.6%), with zircon (up to 17.7%), tourmaline (up to 9.7%), garnet (up to 9.7%), apatite (up to 8.8%), monazite (up to 6.4%), Cr-spinel (up to 3.2%) and sphalerite (up to 2%) (Fig. 8B). Samples NCSb-10, NCSb-13 and NCSa-4 from the overlying Dua Formation (T30) are dominated by translucent heavy minerals which account for c. 90% of the total assemblage. The remaining c. 10% are opaque minerals of which pyrite is the most abundant with traces of hematite, ilmenite, magnetite and jacobsite. The translucent heavy minerals (Fig. 8B) are dominated by rutile (66.8% to 83.3%), with zircon (5.7% to 16.4%), apatite (up to 5.5%), tourmaline (up to 8.9%) and garnet (up to 4.9%), and low proportions or traces of Cr-spinel, monazite, sphalerite, epidote, amphibole, titanite and xenotime. The overlying Thong Formation (T40&50) is again dominated by opaque minerals with abundant pyrite (up to 89.7%) and traces of ilmenite. Translucent heavy minerals form between 10 and 29.1% of the total assemblage. Rutile (up to 47.8%), apatite (up to 26.7%) and tourmaline (up to 20.1%) are the most abundant translucent heavy minerals (Fig. 8b). Zircon (up to 12.1%), sphalerite (5.2%), garnet (up to 5.1%), monazite (2.6%), Cr-spinel (1.1%), titanite (0.7%) and epidote (0.4%) are present in lower proportions (Fig. 8B).

Translucent heavy minerals from the Nam Con Son Basin are generally dominated by ultra-stable minerals, indicated by the high ZTR values (up to c. 98%, Fig. 9B). The youngest analysed unit, the Thong Formation, has the lowest ZTR values (c. 65 to 75%, Fig. 9B) due to the presence of less stable heavy minerals, such as apatite and garnet (Fig. 8b). The other heavy mineral indices are very variable for the Nam Con Son Basin and are best displayed for formations and not individual samples (Fig. 9B) so that trends can be better established. The ATi ratio decreases from the Cau (T20) to the Dua Formation (T30), before increasing in the Thong Formation (T40&50) (Fig. 9B). At the same time the ZTi remains relatively stable and high in the Cau and Dua Formations, before sharply dropping at the top Dua sample and remaining low in the Thong Formation (Fig. 9B). A higher input of garnet in the Thong Formation is indicated by the GZi values of c. 30 (Fig. 9B), higher than in the underlying Dua Formation. The Cau and Dua Formation samples have also ZTi values generally higher than in the overlying Thong Formation. Using ZTR and GZi indices, the three formations are relatively well separated (Fig. 9C).

Effect of baryte removal

Samples CLB2.1, CLB2.3 and NCSb-19 were subjected to the baryte removal technique (Supplementary Table 6). CLB2.1 was analysed in two separates with QEMSCAN. One separate was untreated and the other was treated to remove baryte. 540 translucent heavy mineral grains (excluding carbonates) were identified in the untreated sample with baryte forming 53.7% of the assemblage (Fig. 10A). The treated sample yielded 799 translucent heavy mineral grains with the proportion of baryte decreasing to 20.2% (Fig. 10A). The results from the two separates, after excluding baryte, are almost identical (Fig. 10A) and indicate that the baryte removal technique had no effect on the abundance of other translucent heavy minerals. With the decrease of baryte the count numbers were significantly increased. Anhydrite was not separately counted with QEMSCAN and is listed under other phases in the Supplementary Table 5.

Sample NCSb-19 was also analysed with QEMSCAN in two separates. The untreated sample yielded only 45 translucent heavy minerals with baryte forming 60% of the assemblage (Fig. 10B). The treated sample yielded 559 translucent heavy mineral grains with the proportion of baryte decreasing to 38.5% (Fig. 10B). No apatite and tourmaline were found, reflecting the low number of translucent heavy mineral grains and the high proportion of baryte in the untreated separate, but proportions of other translucent heavy minerals are comparable. The analysis of CLB2.1 and NCSb-19 indicates the importance of baryte removal which results in an increase in the number of other heavy mineral grains and decreases the risk of missing low abundance minerals.

CLB2.3 was analysed with Raman spectroscopy, which also recorded the counts of anhydrite. Seventeen translucent heavy mineral grains were identified (excluding carbonates) from the untreated separate. Baryte and anhydrite each form 17.7% of the assemblage (Fig. 10C). The treated separate

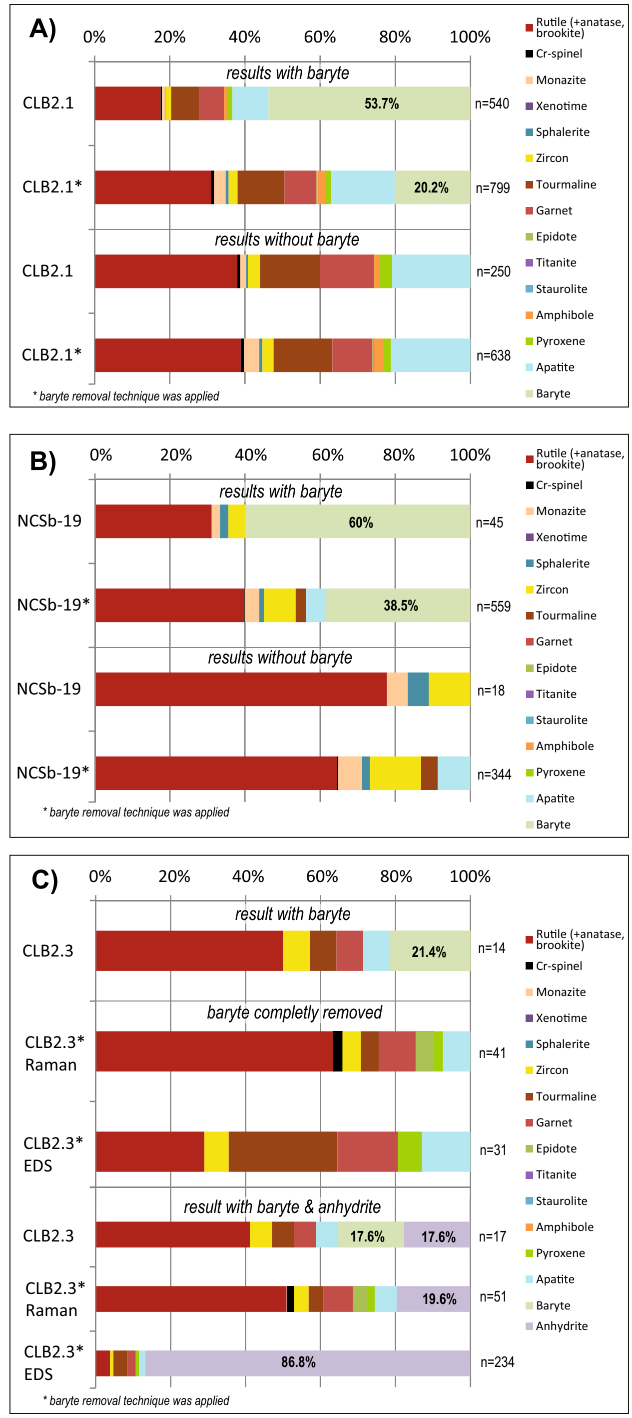

Fig. 10 Comparison of samples treated and untreated for the baryte and anhydrite pulverisation/removal technique, showing the success in reduction of baryte proportions without altering the heavy mineral assemblage. **A**) Sample CLB2.1 shows a baryte reduction from 53.7 to 20.2%. **B**) Sample NCSb-19 shows a baryte reduction of from 60 to 38.5%. **C**) Sample CLB2.3 shows complete removal of baryte. Anhydrite proportions increase in the treated separates, which indicates that further processing and testing is necessary

yielded significantly more translucent heavy mineral grains (51 excluding carbonates). Baryte was not found and, therefore, had been completely removed from the sample, while anhydrite forms 19.6% of the assemblage (Fig. 10C). It is likely that anhydrite was broken down into smaller pieces, but still larger than the 20 µm sieve size. Another treated separate from CLB2.3 was analysed with SEM–EDS, which showed no baryte but abundant anhydrite (Fig. 10C), and suggesting breakdown of larger anhydrite grains into numerous > 20 µm fragments. It is, therefore, concluded that the short vibration time intervals removed the baryte, but for anhydrite removal a longer time interval is required, which requires more testing.

The tested samples showed no significant variations of heavy mineral abundances in treated and untreated samples, indicating that only baryte was removed. Count numbers were increased in the treated samples and identification of some less abundant heavy minerals was possible. For anhydrite contamination, the method is promising, but more tests with different settings need to be conducted.

Discussion

Provenance of the sediments

Cuu Long Basin

The sediments analysed from the Cuu Long Basin were sourced by two different river systems. The first river, which we term the proto-Mekong 1, active from the Oligocene to Early Miocene, deposited the Tra Tan (seismic group D) and Bach Ho (seismic group BI) Formations. These formations have Cretaceous-dominated detrital zircon age populations (Fig. 6), which indicate a proximal Da Lat Zone basement source (Nguyen et al. 2004; Shellnutt et al. 2013; Hennig-Breitfeld et al. 2021). The translucent heavy mineral assemblages vary in the three analysed samples, but relatively low ZTR values are characteristic, with either high proportions of epidote or apatite (Fig. 8A). The zircons are almost entirely Cretaceous, very similar to the onshore Oligocene to Miocene Di Linh Formation (Fig. 11; Hennig et al. 2018). The heavy mineral assemblage of the Di Linh Formation differs from the offshore samples in being rich in ultra-stable grains (Hennig et al. 2018), which might indicate hydraulic sorting or mineral breakdown caused by acid groundwaters on land. Epidote, which is dominant in the Bach Ho samples, was also reported from the Di Linh Formation (Hennig et al. 2018), whereas all other onshore and Cuu Long Basin formations are almost barren of epidote. The lowermost analysed Cuu Long Basin sample CLB9.1 of the Tra Tran Formation has no epidote in contrast to the overlying Bach Ho Formation samples. This implies a fresh epidote-free granitoid source for the older Tra Tran Formation (seismic group D), while the epidote in the Bach Ho Formation samples was derived from altered plagioclase and amphibole in deeper altered granitoids. Hennig-Breitfeld et al. (2021) reported epidote alteration in most onshore granitoids and in associated volcanic rocks, and Jagodziński et al. (2020) reported elevated epidote concentrations in the eastern Mekong River distributaries in the Da Lat Zone and east of the Mekong River Delta from recent deposits, indicating that the Da Lat Zone is a source for epidote.

The overlying Con Son Formation records a major provenance change suggesting input from a different Mekong river in the Middle Miocene. Zircon age populations are dominated by Triassic ages with a few Precambrian grains of c. 800 Ma, c. 1.8 Ga, and 2.5 Ga, as well as Cretaceous and Ordovician–Silurian grains (Fig. 6). The detrital zircon ages are typical of Indochina with a dominance of Triassic Sukhothai arc ages (Sevastjanova et al. 2011; Burrett et al. 2014), but could also indicate a far larger drainage area including the Qiangtang, Yangtze or Songpan–Garze blocks, where similar age spectra are known (Wang et al. 2020 and references therein). Rutile, tourmaline and garnet proportions increase significantly in the Con Son Formation (Fig. 8A), and high proportions of these ultra-stable heavy minerals indicates multi-recycling of metamorphic sources. Mineral ratios GZi, CZi, ZTR also indicate a major source change (Fig. 9A, C). It is unclear exactly when the Con Son Formation was deposited unconformably above the Bach Ho Formation and precisely when this significant source change occurred. Morley et al. (2019) interpret the top of the Bach Ho Formation as c. 20.5 Ma which could be the age of the change. However, the unconformity might have cut down into the underlying Bach Ho Formation during a hiatus in deposition. The rearrangement of the river systems would suggest some period of non-deposition/erosion. Hiep (2017) suggested a Middle Miocene age (starting at c. 16 Ma) for the beginning of deposition of the Con Son Formation. The major unconformity we recognise here, the Bach Ho Unconformity, may, therefore, have an age between 20.5 and 16 Ma. Heavy minerals of the Dong Nai and Con Son formations are very similar, with most heavy mineral indices showing comparable values, but there is also a minor change in zircon ages from the Con Son Formation to the Dong Nai Formation (Fig. 6). Although the provenance remained the same, suggesting the same river system, there is an Eocene zircon population in the Dong Nai Formation indicating an additional source which was not available for the underlying Con Son Formation. The Eocene zircons were probably derived from magmatic rocks in the Da Lat Zone or southern Indochina that were unroofed during the Late Miocene. Fyhn et al. (2010) suggested Palaeocene to Early Eocene inversion in the Phuquoc–Kampot Som Basin, which if associated with magmatism, could be a potential proximal source.

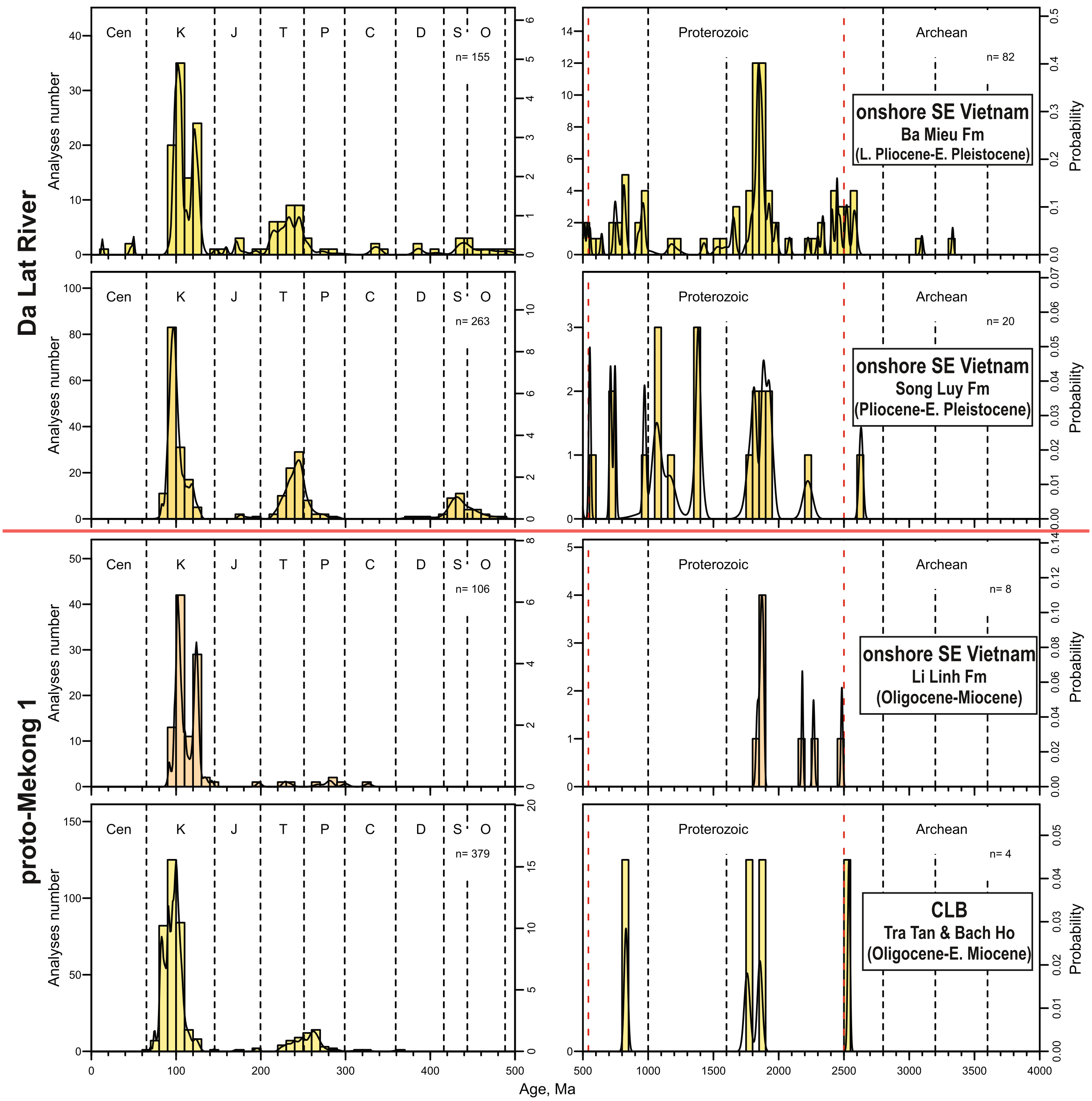

Fig. 11 Detrital zircon age histograms with probability density curves of the lower CLB (Tra Tan, Bach Ho formations) and comparison to the Da Lat Zone sedimentary rocks (data from Hennig et al. 2018). All samples dominated by Cretaceous zircons derived from the Da Lat Zone. The Da Lat River drained into northern Vietnam that results in an increase in Permian–Triassic and Precambrian detrital zircons

Nam Con Son Basin

Three formations were analysed from the Nam Con Son Basin. The Cau (T20) and Dua (T30) formations have very similar heavy mineral assemblages consisting mainly of rutile with zircon, tourmaline, monazite, apatite, and other less abundant minerals, such as garnet or Cr-spinel (Fig. 8B). An assemblage with high ZTR values is usually typical of multi-recycled sedimentary sources. The detrital zircon age populations in both formations are dominated by Permian–Triassic and Paleoproterozoic ages around 1.8–1.9 Ga (Fig. 7). In addition, there are significant Cretaceous, Jurassic, Silurian, Neoproterozoic, and Proterozoic–Archean (c. 2.5 Ga) age populations. The detrital zircon ages suggest similar sources in Indochina, possibly as far as the Qiangtang block. The Cau Formation contains almost twice the number of Phanerozoic detrital zircons compared to Precambrian grains, while the ratio decreases in the Dua Formation to almost equal proportions, and this can be used to distinguish the two formations (Fig. 7). The unconformity between the two formations is here referred to as the Cau Unconformity.

Heavy mineral assemblages from the overlying Thong Formation (T40&50) record another source change. There is a decrease in rutile and an increase of apatite and tourmaline (Fig. 8B). The assemblage is still dominated by ZTR minerals and suggests multi-recycled older sedimentary rocks as source. The detrital zircon age populations are different from the underlying formations (Fig. 7). The dominant age population is Triassic, with only a small population of Permian zircons. The Cretaceous population, previously very prominent, decreases significantly and indicates the Da Lat Zone was no longer an important source. Similarly, the Paleoproterozoic (c. 1.8 to 1.9 Ga) population decreases. Neoproterozoic (especially between 850 to 1000 Ma and at c. 500 Ma) and Proterozoic–Archean (c. 2.5 Ga) zircons increase in the Thong Formation. The Neoproterozoic ages are typical of the Sibumasu terrane of the Malay Peninsula (Hall and Sevastjanova 2012; Lin et al. 2013), especially without the 1.8 Ga population typical of Indochina. Samples from Sibumasu (Hall and Sevastjanova 2012) are also dominated by Triassic detrital zircons with few Permian grains. This suggests that the Thong Formation was directly sourced from the south, where the drainage area included parts of East Malaya and Sibumasu. The Thong Formation is part of the syn-rift 2 phase of the Nam Con Son Basin. The unconformity recognised between the Dua and Thong formations is here named Dua Unconformity. The age of the unconformity is relatively well established, at about 16 Ma, since the underlying Dua Formation was dated in this study as young as 17 Ma and the Thong Formation may be as old as 15.4 Ma (Table 1).

Mekong River evolution

The age of formation of the Mekong River, the source areas of sediments, and the river course through time continue to be debated. Wang et al. (2020) for example used the term paleo-Mekong for an Early Cretaceous river that may have drained the Qiangtang block in a similar way to the present-day Mekong River. However, it is difficult to link the present Mekong River to any Early Cretaceous river in Indochina or South China behind an active Andean-type margin to the east (Shellnutt et al. 2013; Xu et al. 2016; Breitfeld et al. 2017, 2020b; Hennig et al. 2017a, 2017b; Hennig-Breitfeld et al. 2021) when the topography was probably very different. Most researchers discuss the Mekong River evolution from after the Cenozoic India–Asia collision (e.g., Hutchison 1989; Clark et al. 2004; Clift et al. 2006; Zhang et al. 2019), and we focus here on the Oligocene–Miocene to recent development of the Mekong.

Figure 12 illustrates our interpretation of the evolution of the Mekong River using our new provenance data and guided by the present-day major river courses of Indochina and Vietnam. The proto-Mekong 1 (Fig. 12A), of Oligocene to Early Miocene age, is the Phase 1 proto-Mekong named by Hennig et al. (2018) with a delta slightly north of the present-day Mekong River and a tributary flowing from the Da Lat Zone inferred from the Cretaceous-dominated zircon populations of the Tra Tan, Bach Ho and Di Linh formations (Fig. 11), and the immature heavy mineral assemblages of the former two. We suggest that at this time there was no major Mekong River system draining from far to the north in the India–Asia collision zone that supplied sediment to the offshore Vietnam Cuu Long Basin, instead the proto-Mekong 1 with a restricted drainage provided sediment. This is different to some other authors (e.g., Hutchison 1989; Zhang et al. 2019) who have argued a proto- or paleo-Mekong was in place in the Oligo-Miocene draining the Tibetan Plateau. Hutchison (1989) favoured a straight proto-Mekong west of the Khorat Plateau that flowed along the route of the present Chao Phraya River into the Gulf of Thailand before Late Cenozoic faulting changed its course. Brookfield (1998) argued that the proto-Mekong flowed via the Yom River towards the Chao Phraya until river capture in the Late Cenozoic resulted in the present-day Mekong course. Clark et al. (2004) proposed that the Upper Mekong flowed into a paleo-Red River before capture formed the modern Mekong River. None of these rivers with headwaters in the Himalaya or Tibetan Plateau had river courses or delta locations similar to the present-day Mekong River. Clift et al. (2008) modelled several unnamed rivers draining the Tibetan Plateau flowing to the south, and like Hennig et al. (2018), interpreted an early proto-Mekong with drainage restricted to Vietnam. The various proposed courses of the paleo- or proto-Mekong Rivers are discussed in detail in Carling (2009).

At 25 Ma (Fig. 12A) we propose using the term proto-Chao Phraya for the river system identified by Hutchison (1989) and Brookfield (1998) that drained southwards from the India–Asia collision zone towards the Gulf of Thailand/Malay Basin. This river system likely carried sediment to the Nam Con Son Basin. We suggest there were two different strands of the proto-Chao Phraya, a western strand that would become the Salween and an eastern strand which would become the proto-Mekong 2 from the Middle Miocene onwards. This proto-Mekong 2 was formed by capture of the eastern strand of the proto-Chao Phraya by the proto-Mekong 1 (Fig. 12B). The new river had a course similar to the present-day Mekong and drained a large Indochina

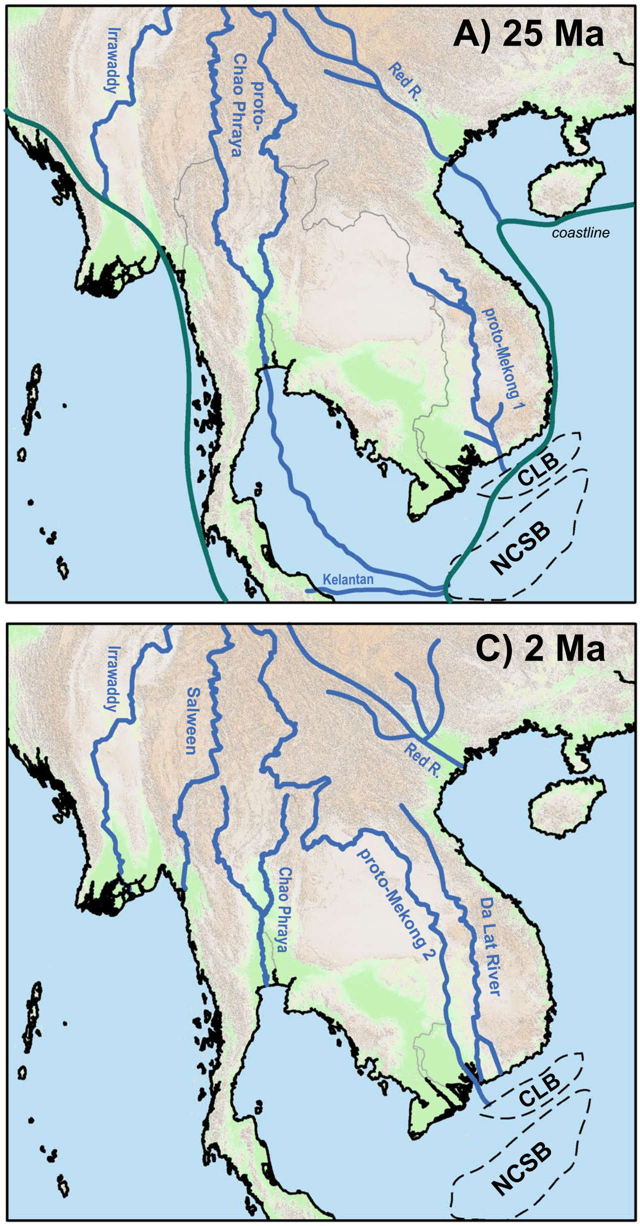

Fig. 12 Drainage reconstruction of the Mekong River using the present-day river courses (marked as grey) as base. **A**) At c. 25 Ma the Proto-Mekong 1 with restricted drainage filled the CLB and the proto-Chao Phraya with two headwater strands draining Indochina and the Himalaya into the NCSB. **B**) Reconstruction at c. 15 Ma the proto-Mekong 1 had expanded and captured the headwaters of the proto-Chao Phraya to form the proto-Mekong 2 with a river course comparable to the present-day Mekong. The Salween may have also been developed at this time. The Chao Phraya with restricted drainage comparable to the present-day was established. **C**) Reconstruction in the Pleistocene, where a northern strand of the proto-Mekong 2 developed into the Da Lat River draining northern Vietnam. **D**) Present-day situation, where the Mekong delta was established south of the Da Lat Zone, bypassing the zone completely

to Himalayan region, consistent with Nie et al. (2018) and Zhang et al. (2019) who also suggested a large proto-Mekong River draining back into the Tibetan Plateau from at least the Mid-Miocene. Detrital zircon age populations from the Con Son and Dong Nai formations (Cuu Long Basin) are very similar to the present-day Mekong zircon signatures (Fig. 13), indicating a similar drainage to that of today. Its delta was likely still in the vicinity of the Da Lat Zone as the present-day Mekong River delta was not formed until the Late Pleistocene to Holocene (e.g. Ta et al. 2002, 2021; Tanabe et al. 2003; Nguyen et al. 2010; Xue et al. 2010; Dung et al. 2013; Thanh et al. 2021). The western strand of the proto-Chao Phraya may have developed into the Salween River in the Middle Miocene leaving a reduced Chao Phraya

(Fig. 12B). The Irrawaddy River (or Ayeyarwady) of Central Myanmar west of the Salween has been in its current geographical position since the late Oligocene, c. 27 Ma (Gough et al. 2020) draining the Indo-Myanmar Ranges in the west and the Eastern Himalayan Syntaxis in the north. The northeast tributary of the proto-Mekong 2 was to become the Da Lat River (Phases 2 and 3 of the proto-Mekong of Hennig et al. 2018) in the Plio-Pleistocene (Fig. 12C) depositing the Ba Mieu and Song Luy formations in the Da Lat Zone. It is unclear what exactly caused the Mekong reorganisation, but Cenozoic uplift (in particular Miocene) of the Khorat Plateau (Mitchell 1986; Racey et al. 1997; Morley 2012) or Late Cenozoic to Pleistocene basalt magmatism associated with uplift in the Da Lat Zone (Rangin et al. 1995; Hoang and Flower 1998; Lee et al. 1998; An et al. 2017) seem to have a major influence at least on the course of the lower Mekong (Fig. 12D).

The fill of the Nam Con Son Basin was not directly linked to the proto-Mekong system. Detrital zircon ages of the Oligocene to Early Miocene Nam Con Son Basin sediments are very similar to the Middle to Late Miocene fills of the Cuu Long Basin (Fig. 13). This suggests that the proto-Chao Phraya (Fig. 12A) which drained from far to the north into the Tibet Plateau fed sediment into the Nam Con Son Basin before the Middle Miocene via the then fluvial area of the Gulf of Thailand (Fig. 12A). After the Dua Unconformity in the Middle Miocene the Nam Con Son Basin was filled mainly by the Kelantan River (Fig. 12B), which drained back into Sibumasu. The interpretation that the Pleistocene fill of the Nam Con Son Basin was derived from a prograding paleo-Mekong (e.g. Matthews et al. 1997), therefore, seems unlikely. Figure 14A illustrates the paleogeography of the southern South China Sea region in the late Oligocene before the Bach Ho and Dua unconformities, and Fig. 14B after the unconformities in the Middle Miocene with the major river courses. The results of this study support the interpretation of Hennig et al. (2018) of a major mid-Miocene unconformity in southern Vietnam and Indochina at which the drainage network was reorganised.

Detrital zircon age comparison of the proto-Mekong(s) with the proto-Chao Phraya

The MDS plot (Fig. 15) of the detrital zircon age data from this study compared to the present-day Mekong data (Bodet and Schärer 2000; Clift et al. 2006; Nguyen et al. 2018) and the onshore Da Lat Zone sedimentary rocks (Hennig et al. 2018), shows the evolution of the different systems and their similarities by scaling the data of samples/formations into two dimensions (Vermeesch 2013) for a faster visual representation. The Oligocene to Early Miocene fill of the Cuu Long Basin (Tra Tan, Bach Ho formations) was derived from the proto-Mekong 1, which had a localised drainage of the Da Lat Zone and a river delta along the SE Vietnam coastline directly adjacent to the Cuu Long Basin. The onshore Di Linh Formation represents the last onshore remains of this system. This fill of the Cuu Long Basin is estimated to be as thick as c. 4000 m (Cuong and Warren 2009) and indicates that despite the restricted drainage, large amounts of material were eroded and deposited by the proto-Mekong 1. In contrast, the Middle to Late Miocene Cuu Long Basin sediments (Con Son and Dong Nai formations) resemble the present-day Mekong deposits in their detrital zircon age populations and were part of the proto-Mekong 2 system (Figs. 13, 15). The Cretaceous population in both formations, and the Jurassic zircon population in the Con Son Formation indicate a slightly different drainage compared to the present-day, probably involving some minor input from the Da Lat Zone that is by-passed by the present-day Mekong (Fig. 12B). The Cretaceous-dominated proto-Mekong 1 age distribution signature is illustrated in Fig. 11. Noticeable in the histograms is that the offshore formations have a wide Late Cretaceous age peak from c. 80 to 110 Ma, while the Di Linh Formation has a bimodal Cretaceous age distribution, suggesting local igneous bodies had strong influence on the age distribution. The offshore samples have also a slight population in the Permian–Triassic, which is almost absent in the Di Linh sample that suggests input of older basement in the vicinity of the delta (e.g., Chau Thoi). The Da Lat River developed its drainage towards the north in the Pliocene, resulting in an increase of Triassic and Precambrian zircons derived from Indochina and South China basement (Fig. 11; Hennig et al. 2018). The Ba Mieu and Song Luy formations deposited by the Da Lat River (Phase 2 and 3 of the proto-Mekong in Hennig et al. 2018) are clearly distinguishable from the proto-Mekong 1 and the proto-Mekong 2/proto-Chao Phraya by their detrital zircon ages (Figs. 11 and 15).

The lower Nam Con Son Basin successions (Cau/T20 and Dua formations/T30) are also very similar to the upper Cuu Long Basin samples (Fig. 15), especially the Cau Formation, indicating a similar provenance and supporting the suggestion that the headwaters of the proto-Chao Phraya would later become the proto-Mekong 2. The heavy mineral assemblages are mineralogically comparable, but mineral proportions in the Cuu Long Basin and Nam Con Son Basin samples vary, possibly as a result of sorting. Garnet is relatively abundant in the Cuu Long Basin but present only in low amounts in the Cau and Dua formations of the Nam Con Son Basin. The Cretaceous zircons in the Cau and Dua formations (Figs. 7 and 13) were likely sourced by highs at the basin margin (e.g. Con Son Swell) rather than input from the Da Lat Zone. The overlying Thong Formation (T40&50) has small differences in detrital zircon ages that is represented by being slightly off T20 and T30 (Fig. 15), and has also a slightly different heavy mineral assemblage

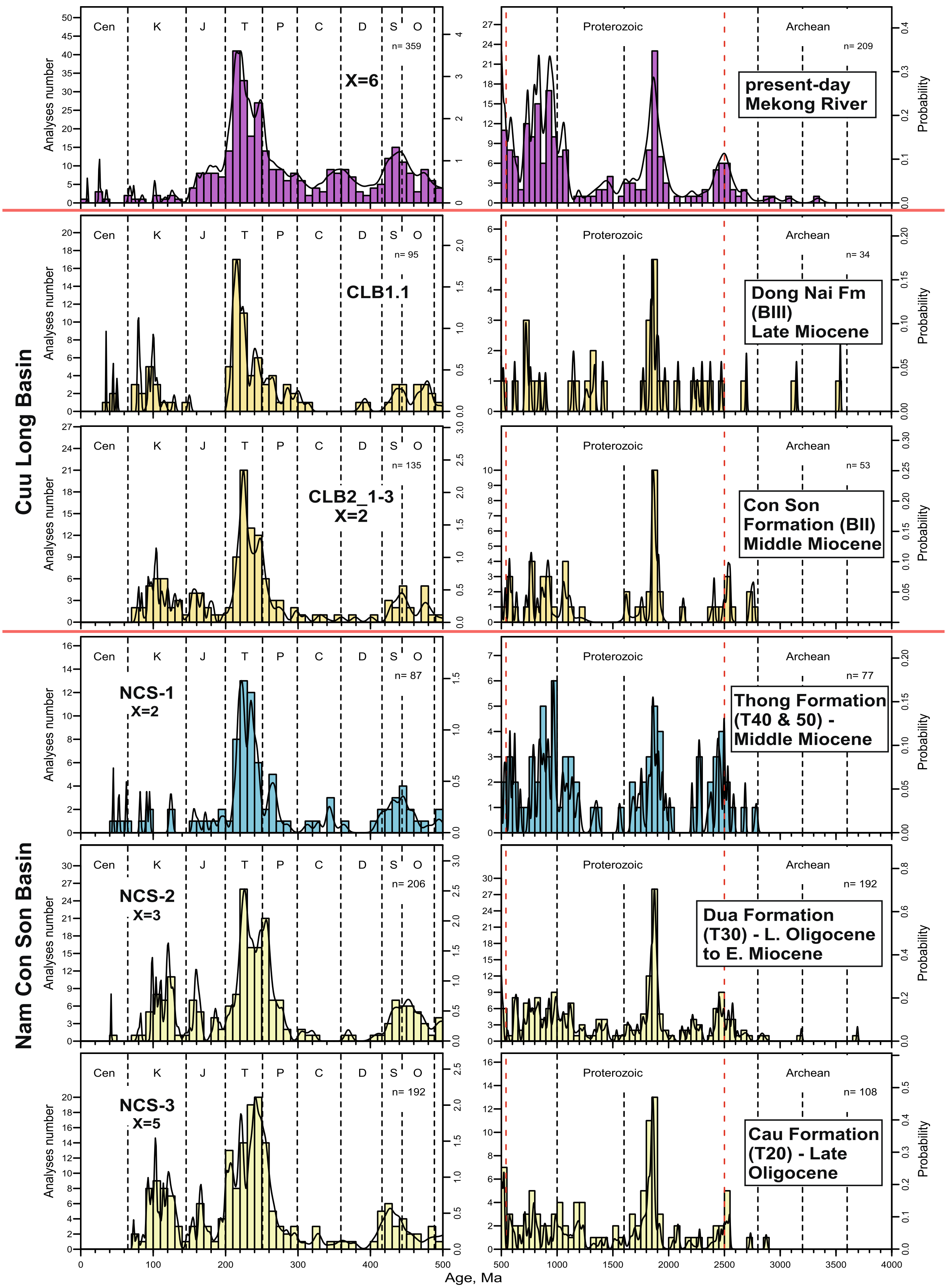
Cuu Long Basin
Nam Con Son Basin
Analyses number
Probability
Cen K J T P C D S O
Proterozoic
Archean
X=6
n= 359
n= 209
present-day Mekong River
CLB1.1
n= 95
n= 34
Dong Nai Fm (BIII) Late Miocene
CLB2_1-3 X=2
n= 135
n= 53
Con Son Formation (BII) Middle Miocene
NCS-1 X=2
n= 87
n= 77
Thong Formation (T40 & 50) - Middle Miocene
NCS-2 X=3
n= 206
n= 192
Dua Formation (T30) - L. Oligocene to E. Miocene
NCS-3 X=5
n= 192
n= 108
Cau Formation (T20) - Late Oligocene
Age, Ma

◂**Fig. 13** Detrital zircon age histograms with probability density curves of samples with heterogeneous, Triassic-dominated age peaks (CLB: Con Son, Dong Nai formations; NCSB: Cau, Dua, Thong formations) and comparison to the present-day Mekong River (data from Bodet and Schärer 2000; Clift et al. 2006; Nguyen et al. 2018)

(Fig. 8B). The increase in Cambrian and Neoproterozoic zircons (Figs. 7 and 13) is a typical Sibumasu signature, indicating a southwestern source in the Malay Peninsula drained by the Kelantan River. A similar drainage for the Nam Con Son Basin fill was concluded by Morley et al. (2011) and Morley and Morley (2013).

Conclusions

Detrital zircon ages and heavy mineral assemblages of Cenozoic sedimentary formations in on- and offshore SE Vietnam can be used to reconstruct the drainage history of major river systems in Indochina. The Oligocene to Early Miocene basin fill of the Cuu Long Basin (Tra Tan and Bach Ho formations) was derived almost entirely from uplifted Dal Lat Zone basement highs along the basin margin by the proto-Mekong 1. The Bach Ho Unconformity marks a major source change and the overlying Con Son and Dong Nai formations have a provenance similar to the present-day Mekong, indicating that by the Early–Middle Miocene boundary the proto-Mekong 2 had a course similar to the present-day. The proto-Mekong 1 captured the headwaters of the proto-Chao Phraya to form the proto-Mekong 2. The Oligocene to Early Miocene basin fill of the Nam Con Son Basin (Cau and Dua formations) has detrital zircon ages that resemble the present-day Mekong and the upper Cuu Long Basin fill, suggesting a similar provenance. We propose that in the Oligocene to Early Miocene a proto-Chao Phraya, with a drainage area into the Himalaya highlands, filled the Nam Con Son Basin. The Thong Formation of the Nam Con Son Basin, unconformable on top of the Dua Formation, has a partly Sibumasu provenance and suggests input from the Malay–Thai Peninsula. The proto-Mekong 1 and 2 did not

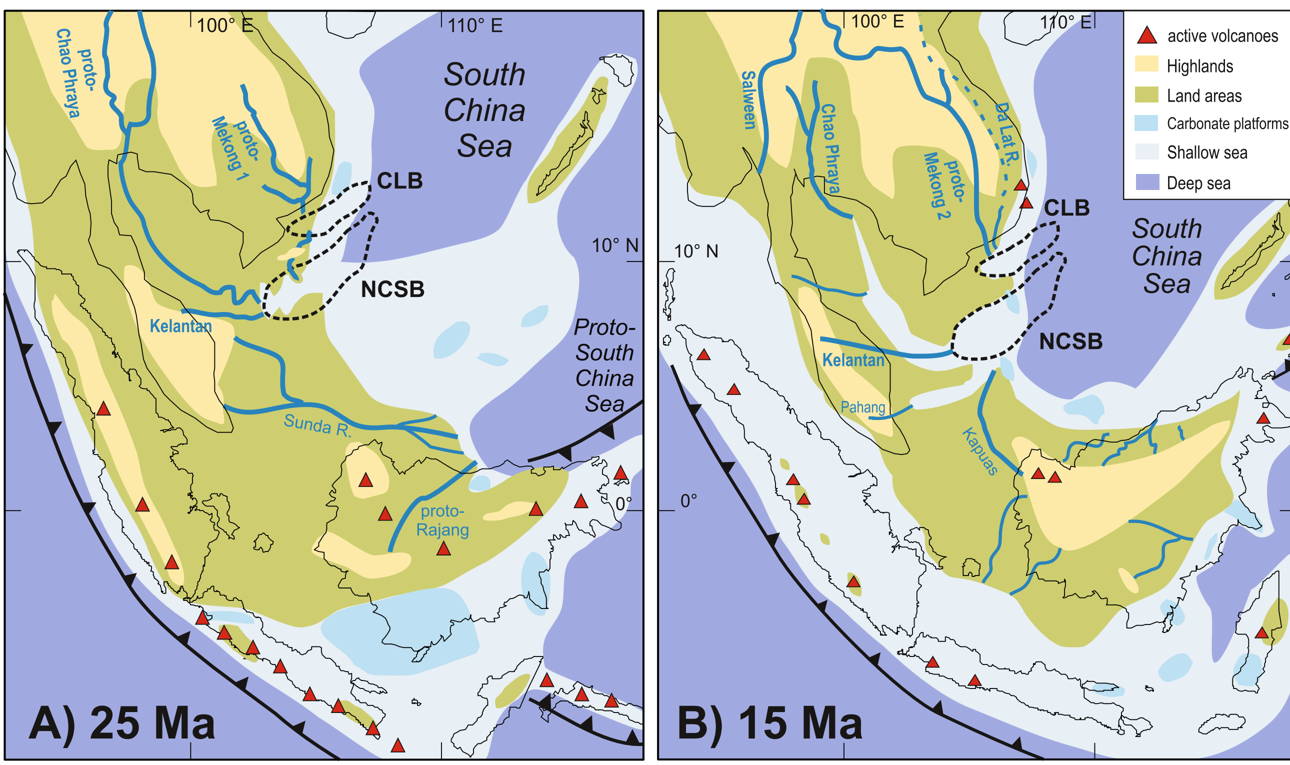

Fig. 14 Paleogeography maps and reconstruction of the proto-Mekong River course during the two crucial time intervals (modified from Hall 2013; Morley and Morley 2013; Hennig-Breitfeld et al. 2019; Breitfeld et al. 2020a). **A**) Reconstruction at c. 25 Ma before the Bach Ho and Dua unconformities. The CLB is filled by the proto-Mekong 1 with a drainage area of the Da Lat Zone. The proto-Chao Phraya with the Kelantan filled the NCSB with the Gulf of Thailand being a fluvial–lacustrine area. The Sunda River drains the Sunda Shelf and had its delta in the NW Borneo region (based on Hennig-Breitfeld et al. 2019; Breitfeld et al. 2020a). **B**) Reconstruction at c. 15 Ma after the major drainage reorganisation. Proto-Mekong 1 has captured headwaters of proto-Chao Phraya to form the proto-Mekong 2 with a similar provenance and river course as the present-day that fills the CLB. The Kelantan fills the NCSB from the Malay–Thai Peninsula. The Da Lat River in SE Vietnam may begin to develop from the northern strand of the former proto-Mekong 1. The headwaters of the proto-Chao Phraya were captured, leaving a Chao Phraya with restricted drainage similar to the present-day

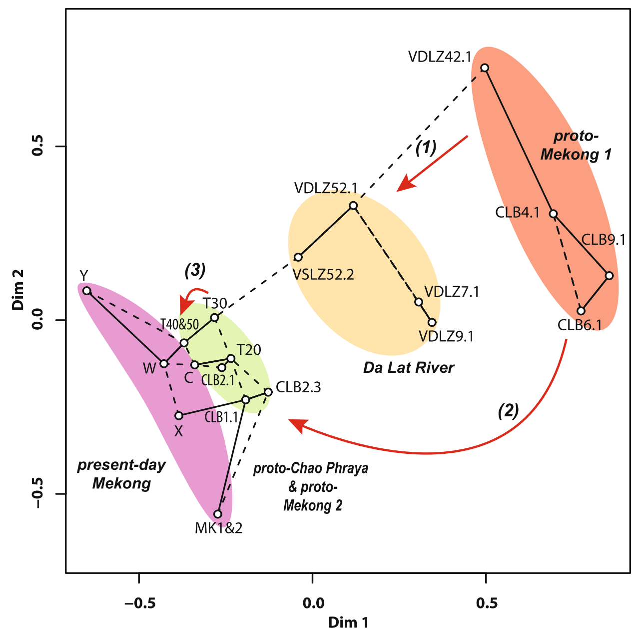

Fig. 15 MDS plots of detrital zircon data (Vermeesch 2013; Vermeesch et al. 2016) of the CLB and NCSB data (this study); onshore Da Lat Zone data: VDLZ42.1-Di Linh Formation, VDLZ7.1 and VDLZ9.1 Song Luy Formation, and VDLZ52.1 and VDLZ52.2 Ba Mieu Formation (from Hennig et al. 2018); and present-day Mekong: MK1&2 (Bodet and Schärer 2000), C (Clift et al. 2006); X, Y and W (Nguyen et al. 2018). Red-shaded area symbolises the Oligocene to Lower Miocene proto-Mekong 1 (D/BI Tra Tan and Bach Ho of CLB, and onshore Di Linh Formation). Yellow-shaded area represents the Plio-Pleistocene Da Lat River (onshore Song Luy and Ba Mieu formations). The green-shaded area represents the proto-Chao Phraya before (NCSB T20/30 Cau and Dua) and the proto-Mekong 2 after capture (CLB BII/BIII Con Son and Dong Nai) by the proto-Mekong 1, as well as the Kelantan signal (NCSB T40&50 Thong). The purple area represents the present-day Mekong. Arrow 1: represents the evolution from proto-Mekong 1 to Da Lat River (Phase 2 and 3 proto-Mekong in Hennig et al. 2018), arrow 2: represents the capture of the proto-Chao Phraya headwaters by proto-Mekong 1 to form the proto-Mekong 2, and 3: the change from Indochina sources for the T20/30 to Sibumasu source for T40&50 in the NCSB. The MDS plots are not sufficient to distinguish clearly between the Sibumasu–Indochina (Thong Formation) and the Indochina–Qiangtang provenance (Cau, Dua, Con Son, Dong Nai formations, present-day Mekong). Supplementary Figure 4 illustrates the same plot with NCSB samples separately plotted. Lines represent nearest neighbour. Source data for the MDS plot can be found in Supplementary Table 7

provide sediment to the Nam Con Son Basin. In both basins unconformities around the Early to Miocene boundary (20.5 to 16 Ma for the Cuu Long Basin Bach Ho Unconformity and 17 to 15.4 Ma for the Nam Con Son Basin Dua Unconformity) are marked by a major source change associated with a drainage reorganisation.

Supplementary Information The online version contains supplementary material available at https://doi.org/10.1007/s00531-022-02214-0.

Acknowledgements The project was funded by the SE Asia Research Group, which is sponsored by a consortium of industry bodies. Talisman Vietnam (now Repsol Vietnam) is thanked for financial support, sample shipment and geological background. Tim Pearce of Chemostrat Ltd. is thanked for support on a number of additional heavy mineral Raman spectroscopy analyses. We thank Martin Rittner and Andy Carter for help with the LA–ICP–MS analysis at UCL/Birkbeck College (UK). Jenny Omma of Rocktype is kindly acknowledged for the QEMSCAN results. Many thanks also to the South Vietnam Geological Mapping Division, in particular Dinh Quang Sang, Mai Kim Vinh and Trinh Van Long, for the insightful discussions in the field and help with the sample logistics. Ulrich Riller is thanked for editorial assistance, and topic editor Nora Noffke, Clive Burrett and an anonymous reviewer are thanked for comments on the manuscript.

Funding Open Access funding enabled and organized by Projekt DEAL.

References

An A-R, Choi SH, Yu Y, Lee D-C (2017) Petrogenesis of Late Cenozoic basaltic rocks from southern Vietnam. Lithos 272:192–204. https://doi.org/10.1016/j.lithos.2016.12.008

Andersen T (2002) Correction of common lead in U-Pb analyses that do not report ^{204}Pb. Chem Geol 192:59–79. https://doi.org/10.1016/S0009-2541(02)00195-X

Andò S, Bersani D, Vignola P, Garzanti E (2009) Raman spectroscopy as an effective tool for high-resolution heavy-mineral analysis: examples from major Himalayan and Alpine fluvio-deltaic systems. Spectrochim Acta Part A Mol Biomol Spectrosc 73:450–455. https://doi.org/10.1016/j.saa.2008.11.005

Andò S, Garzanti E (2014) Raman spectroscopy in heavy-mineral studies. Geol Soc Spec Publ 386:395–412. https://doi.org/10.1144/SP386.2

Areshev EG, Dong TL, San NT, Shnip OA (1992) Reservoirs in fractured basement on the continental shelf of southern Vietnam. J Pet Geol 15:451–464. https://doi.org/10.1111/j.1747-5457.1992.tb01045.x

Barckhausen U, Engels M, Franke D, Ladage S, Pubellier M (2014) Evolution of the South China Sea: Revised ages for breakup and seafloor spreading. Mar Pet Geol 58:599–611. https://doi.org/10.1016/j.marpetgeo.2014.02.022

Basori MBI, Leman MS, Zaw K, Meffre S, Large RR, Mohamed KR, Makoundi C, Mohd Zin M (2018) Implications of U-Pb detrital zircon geochronology analysis for the depositional age, provenance, and tectonic setting of continental Mesozoic formations in the East Malaya Terrane, Peninsular Malaysia. Geol J 53:2908–2917. https://doi.org/10.1002/gj.3131

Bat D, Quynh H, Que P, Dong T (1993) Tertiary stratigraphy of continental shelf of Vietnam, First International Seminar on

the Stratigraphy of the Southern Continental Shelf of Vietnam, Hanoi
Bodet F, Schärer U (2000) Evolution of the SE-Asian continent from U-Pb and Hf isotopes in single grains of zircon and baddeleyite from large rivers. Geochim Cosmochim Acta 64:2067–2091. https://doi.org/10.1016/S0016-7037(00)00352-5
BouDagher-Fadel MK (2015) Biostratigraphic and Geological Significance of Planktonic Foraminifera, 2nd edn. UCL Press, London
Boudagher-Fadel MK (2018a) Evolution and geological significance of larger benthic foraminifera. UCL Press, London
Boudagher-Fadel MK (2018b) Revised diagnostic first and last occurrences of Mesozoic and Cenozoic planktonic foraminifera. UCL Office of the Vice-Provost Research, Professional Papers Series, 1–5
Breitfeld HT, Davies L, Hall R, Armstrong R, Forster M, Lister G, Thirlwall M, Grassineau N, Hennig-Breitfeld J, van Hattum MW (2020a) Mesozoic Paleo-Pacific subduction beneath SW Borneo: U-Pb geochronology of the Schwaner granitoids and the Pinoh Metamorphic Group. Front Earth Sci 8:568715. https://doi.org/10.3389/feart.2020.568715
Breitfeld HT, Hall R (2018) The eastern Sundaland margin in the latest Cretaceous to Late Eocene: Sediment provenance and depositional setting of the Kuching and Sibu Zones of Borneo. Gondwana Res 63:34–64. https://doi.org/10.1016/j.gr.2018.06.001
Breitfeld HT, Hall R, Galin T, Forster MA, BouDagher-Fadel MK (2017) A Triassic to Cretaceous Sundaland-Pacific subduction margin in West Sarawak, Borneo. Tectonophysics 694:35–56. https://doi.org/10.1016/j.tecto.2016.11.034
Breitfeld HT, Hennig-Breitfeld J, BouDagher-Fadel MK, Hall R, Galin T (2020b) Oligocene-Miocene drainage evolution of NW Borneo: Stratigraphy, sedimentology and provenance of Tatau-Nyalau province sediments. J Asian Earth Sci 195:104331. https://doi.org/10.1016/j.jseaes.2020.104331
Briais A, Patriat P, Tapponnier P (1993) Updated interpretation of magnetic anomalies and seafloor spreading stages in the South China Sea: Implications for the Tertiary tectonics of Southeast Asia. Journal of Geophysical Research: Solid Earth 98:6299–6328
Brookfield ME (1998) The evolution of the great river systems of southern Asia during the Cenozoic India-Asia collision: rivers draining southwards. Geomorphology 22:285–312. https://doi.org/10.1016/S0169-555X(97)00082-2
Burley SD, Breitfeld HT, Morley RJ, Kassan J, Sukarno M, Wantoro DW (2021) A tuffaceous volcaniclastic turbidite bed of Early Miocene age in the Temburong Formation of Labuan, North-West Borneo and its implications for the Proto-South China Sea subduction in the Burdigalian. Depos Rec 7:111–146. https://doi.org/10.1002/dep2.132
Burrett C, Zaw K, Meffre S, Lai CK, Khositanont S, Chaodumrong P, Udchachon M, Ekins S, Halpin J (2014) The configuration of Greater Gondwana—evidence from LA ICPMS, U-Pb geochronology of detrital zircons from the Palaeozoic and Mesozoic of Southeast Asia and China. Gondwana Res 26:31–51. https://doi.org/10.1016/j.gr.2013.05.020
Cao L, Jiang T, Wang Z, Zhang Y, Sun H (2015) Provenance of upper miocene sediments in the yinggehai and qiongdongnan basins, Northwestern South China Sea: evidence from REE, heavy minerals and zircon U-Pb ages. Mar Geol 361:136–146. https://doi.org/10.1016/j.margeo.2015.01.007
Carling PA (2009) Chapter 2 - The Geology of the Lower Mekong River. In: Campbell IC (ed) The Mekong. Academic Press, San Diego, pp 13–28
Chang J-H, Lee T-Y, Hsu H-H, Liu C-S (2015) Comment on Barckhausen et al., 2014–Evolution of the South China Sea: Revised ages for breakup and seafloor spreading. Mar Pet Geol 59:676–678. https://doi.org/10.1016/j.marpetgeo.2014.09.003
Clark M, Schoenbohm L, Royden L, Whipple K, Burchfiel B, Zhang X, Tang W, Wang E, Chen L (2004) Surface uplift, tectonics, and erosion of eastern Tibet from large-scale drainage patterns. Tectonics. https://doi.org/10.1029/2002TC001402
Clift PD, Carter A, Campbell IH, Pringle MS, Van Lap N, Allen CM, Hodges KV, Tan MT (2006) Thermochronology of mineral grains in the Red and Mekong Rivers, Vietnam: provenance and exhumation implications for Southeast Asia. Geochem Geophys Geosyst 7:Q10005. https://doi.org/10.1029/2006GC001336
Clift PD, Long HV, Hinton R, Ellam RM, Hannigan R, Tan MT, Blusztajn J, Duc NA (2008) Evolving east Asian river systems reconstructed by trace element and Pb and Nd isotope variations in modern and ancient Red River-Song Hong sediments. Geochem Geophys Geosyst 9:Q04039. https://doi.org/10.1029/2007GC001867
Cohen KM, Finney SC, Gibbard PL, Fan J-X (2013) The ICS international chronostratigraphic chart. Episodes 36:199–204
Cuong TX, Warren JK (2009) Bach ho field, a fractured granitic basement reservoir, Cuu Long Basin, offshore SE Vietnam: a "buried-hill" play. J Pet Geol 32:129–156. https://doi.org/10.1111/j.1747-5457.2009.00440.x
Dien P, Tai P, Dzung L, Tiem P, Nhuan D (1998) Late-Mesozoic and Early Cenozoic events and petroleum system of the Cuu Long Basin. PetroVietnam Review 1:4–23
Dodd TJ, Gillespie MR, Leslie AG, Kearsey TI, Kendall RS, Bide TP, Dobbs MR, Millar IL, Lee MKW, Chiam K (2019) Paleozoic to Cenozoic sedimentary bedrock geology and lithostratigraphy of Singapore. J Asian Earth Sci 180:103878. https://doi.org/10.1016/j.jseaes.2019.103878
Dung BV, Tuan HA, Van Kieu N, Man HQ, Thuy NTT, Huyen PTD (2018) Depositional environment and reservoir quality of Miocene sediments in the central part of the Nam Con Son basin, Southern Vietnam shelf. Mar Pet Geol 97:672–689. https://doi.org/10.1016/j.marpetgeo.2018.05.004
Dung N, Merz B, Bárdossy A, Apel H (2013) Flood hazard in the Mekong Delta—a probabilistic, bivariate, and non-stationary analysis with a short-termed future perspective. Natural Hazards and Earth System Sciences Discussions 1:275–322. https://doi.org/10.5194/nhessd-1-275-2013
Dunkl I, von Eynatten H, Andò S et al (2020) Comparability of heavy mineral data—The first interlaboratory round robin test. Earth Sci Rev 211:103210. https://doi.org/10.1016/j.earscirev.2020.103210
Franke D, Savva D, Pubellier M, Steuer S, Mouly B, Auxietre J-L, Meresse F, Chamot-Rooke N (2014) The final rifting evolution in the South China Sea. Mar Pet Geol 58:704–720. https://doi.org/10.1016/j.marpetgeo.2013.11.020
Fyhn MB, Boldreel LO, Nielsen LH (2009) Geological development of the Central and South Vietnamese margin: Implications for the establishment of the South China Sea, Indochinese escape tectonics and Cenozoic volcanism. Tectonophysics 478:184–214. https://doi.org/10.1016/j.tecto.2009.08.002
Fyhn MB, Green PF, Bergman SC, Van Itterbeeck J, Tri TV, Dien PT, Abatzis I, Thomsen TB, Chea S, Pedersen SA (2016) Cenozoic deformation and exhumation of the Kampot Fold Belt and implications for south Indochina tectonics. Journal of Geophysical Research: Solid Earth 121:5278–5307. https://doi.org/10.1002/2016JB012847
Fyhn MB, Pedersen SA, Boldreel LO, Nielsen LH, Green PF, Dien PT, Huyen LT, Frei D (2010) Palaeocene–early Eocene inversion of the Phuquoc-Kampot Som Basin: SE Asian deformation associated with the suturing of Luconia. J Geol Soc 167:281–295. https://doi.org/10.1144/0016-76492009-039
Fyhn MB, Thomsen TB, Keulen N, Knudsen C, Rizzi M, Bojesen-Koefoed J, Olivarius M, Tri TV, Phach PV, Minh NQ (2019) Detrital

zircon ages and heavy mineral composition along the Gulf of Tonkin-implication for sand provenance in the Yinggehai-Song Hong and Qiongdongnan basins. Mar Pet Geol 101:162–179. https://doi.org/10.1016/j.marpetgeo.2018.11.051

Galin T, Breitfeld HT, Hall R, Sevastjanova I (2017) Provenance of the Cretaceous-Eocene Rajang Group submarine fan, Sarawak, Malaysia from light and heavy mineral assemblages and U-Pb zircon geochronology. Gondwana Res 51:209–233. https://doi.org/10.1016/j.gr.2017.07.016

Gong L, Hollings P, Zhang Y, Tian J, Li D, Berador AE, Chen H (2021) Contribution of an Eastern Indochina-derived fragment to the formation of island arc systems in the Philippine Mobile Belt. GSA Bull 133:1979–1995. https://doi.org/10.1130/B35793.1

Gough A, Hall R, BouDagher-Fadel MK (2020) Mid-Cenozoic fluvio-deltaic to marine environments of the Salin Sub-basin, Central Myanmar. J Asian Earth Sci 190:104143. https://doi.org/10.1016/j.jseaes.2019.104143

Gradstein FM, Ogg JG, Schmitz MD, Ogg GM (2012) The geologic time scale 2012. Elsevier, Amsterdam

Griffin WL, Powell WJ, Pearson NJ, O'Reilly SY (2008) GLITTER: data reduction software for laser ablation ICP-MS. In: Sylvester PJ (ed) Laser Ablation-ICP-MS in the Earth Sciences: Current Practices and Outstanding Issues. Mineralogical Association of Canada, short course series 40, pp 308–311

Hall R (2013) Contraction and extension in northern Borneo driven by subduction rollback. J Asian Earth Sci 76:399–411. https://doi.org/10.1016/j.jseaes.2013.04.010

Hall R, Morley CK (2004) Sundaland Basins. Continent-Ocean Interactions within East Asian Marginal Seas 149:55–85. https://doi.org/10.1029/149GM04

Hall R, Sevastjanova I (2012) Australian crust in Indonesia. Aust J Earth Sci 59:827–844. https://doi.org/10.1080/08120099.2012.692335

Hayes DE, Nissen SS (2005) The South China sea margins: Implications for rifting contrasts. Earth Planet Sci Lett 237:601–616. https://doi.org/10.1016/j.epsl.2005.06.017

Hennig J, Breitfeld HT, Gough A, Hall R, Long TV, Kim VM, Quang SD (2018) U-Pb zircon ages and provenance of upper Cenozoic sediments from the Da Lat Zone, SE Vietnam: implications for an intra-Miocene unconformity and paleo-drainage of the proto-Mekong River. J Sediment Res 88:495–515. https://doi.org/10.2110/jsr.2018.26

Hennig J, Breitfeld HT, Gough A, Hall R, Trinh VL, Mai VK, Dinh SQ (2017a). SE Vietnam U-Pb zircon ages and provenance: Correlating the Da Lat Zone on land with the Cuu Long Basin offshore, AGU Fall Meeting Abstracts, New Orleans, EP21A-1830.

Hennig J, Breitfeld HT, Hall R, Nugraha AMS (2017b) The Mesozoic tectono-magmatic evolution at the Paleo-Pacific subduction zone in West Borneo. Gondwana Res 48:292–310. https://doi.org/10.1016/j.gr.2017.05.001

Hennig-Breitfeld J, Breitfeld HT, Hall R, BouDagher-Fadel M, Thirlwall M (2019) A new upper Paleogene to Neogene stratigraphy for Sarawak and Labuan in northwestern Borneo: Paleogeography of the eastern Sundaland margin. Earth Sci Rev 190:1–32. https://doi.org/10.1016/j.earscirev.2018.12.006

Hennig-Breitfeld J, Breitfeld HT, Sang DQ, Vinh MK, Van Long T, Thirlwall M, Cuong TX (2021) Ages and character of igneous rocks of the Da Lat Zone in SE Vietnam and adjacent offshore regions (Cuu Long and Nam Con Son basins). J Asian Earth Sci 218:104878. https://doi.org/10.1016/j.jseaes.2021.104878

Hiep N (2017) The Petroleum Geology and Resources of Vietnam, 2nd edn. Science and Technics Publishing House, Hanoi

Hoang N, Flower M (1998) Petrogenesis of Cenozoic basalts from Vietnam: implication for origins of a 'diffuse igneous province.' J Petrol 39:369–395. https://doi.org/10.1093/petroj/39.3.369

Hubert JF (1962) A zircon-tourmaline-rutile maturity index and the interdependence of the composition of heavy mineral assemblages with the gross composition and texture of sandstones. J Sediment Petrol 32:440–450. https://doi.org/10.1306/74D70CE5-2B21-11D7-8648000102C1865D

Hung ND, Le HV (2004) Petroleum Geology of Cuu Long Basin-Offshore Vietnam. AAPG Search and Discovery article 10062

Hutchison CS (1989) Geological evolution of South-east Asia. Clarendon Press, Oxford

Jagodziński R, Sternal B, Stattegger K, Szczuciński W (2020) Sediment distribution and provenance on the continental shelf off the Mekong River, SE Vietnam: Insights from heavy mineral analysis. J Asian Earth Sci 196:104357. https://doi.org/10.1016/j.jseaes.2020.104357

Jiang T, Cao L, Xie X, Wang Z, Li X, Zhang Y, Zhang D, Sun H (2015) Insights from heavy minerals and zircon U-Pb ages into the middle Miocene-Pliocene provenance evolution of the Yinggehai Basin, northwestern South China Sea. Sed Geol 327:32–42. https://doi.org/10.1016/j.sedgeo.2015.07.011

Lafuente B, Downs RT, Yang H, Stone N (2016) 1. The power of databases: The RRUFF project. In: Armbruster T, Danisi RM (eds) Highlights in mineralogical crystallography. De Gruyter (O), pp 1–30

Larsen HC, Mohn G, Nirrengarten M, Sun Z, Stock J, Jian Z, Klaus A, Alvarez-Zarikian C, Boaga J, Bowden S (2018) Rapid transition from continental breakup to igneous oceanic crust in the South China Sea. Nat Geosci 11:782–789. https://doi.org/10.1038/s41561-018-0198-1

Lee GH, Lee K, Watkins JS (2001) Geologic evolution of the Cuu Long and Nam Con Son basins, offshore southern Vietnam, South China Sea. AAPG Bull 85:1055–1082. https://doi.org/10.1306/8626CA69-173B-11D7-8645000102C1865D

Lee TY, Lo CH, Chung SL, Chen CY, Wang PL, Lin WP, Hoang N, Chi CT, Yem NT (1998) $^{40}Ar/^{39}Ar$ dating result of Neogene basalts in Vietnam and its tectonic implication. Mantle Dynamics and Plate Interactions in East Asia 27:317–330. https://doi.org/10.1029/GD027p0317

Lin Y-L, Yeh M-W, Lee T-Y, Chung S-L, Iizuka Y, Charusiri P (2013) First evidence of the Cambrian basement in Upper Peninsula of Thailand and its implication for crustal and tectonic evolution of the Sibumasu terrane. Gondwana Res 24:1031–1037. https://doi.org/10.1016/j.gr.2013.05.014

Liu Q, Zhu H, Shu Y, Zhu X, Yang X, Chen L, Tan M, Geng M (2016) Provenance identification and sedimentary analysis of the beach and bar systems in the Palaeogene of the Enping Sag, Pearl River Mouth Basin, South China Sea. Mar Pet Geol 70:251–272. https://doi.org/10.1016/j.marpetgeo.2015.12.002

Liu S, Lu P, Liu D, Jin P, Wang W (2009) Pinpointing the sources and measuring the lengths of the principal rivers of the world. Int J Digit Earth 2:80–87. https://doi.org/10.1080/17538940902746082

Mange MA, Maurer HFW (1992) Heavy minerals in colour. Chapman & Hall, London

Matthews SJ, Fraser AJ, Lowe S, Todd SP, Peel FJ (1997) Structure, stratigraphy and petroleum geology of the SE Nam Con Son Basin, offshore Vietnam. Geol Soc Spec Publ 126:89–106. https://doi.org/10.1144/GSL.SP.1997.126.01.07

Meyer K (2012) Nam Con Son Basin analysis: the old and new. International Petroleum Technology Conference, European Association of Geoscientists & Engineers, Bangkok, Thailand, 14470

Mitchell AHG (1986) Mesozoic and Cenozoic regional tectonics and metallogenesis in Mainland SE Asia. Geol. Soc Malaysia, Bulletin 20:221–239. https://doi.org/10.7186/bgsm20198612

Morley C (2012) Late Cretaceous–early Palaeogene tectonic development of SE Asia. Earth Sci Rev 115:37–75. https://doi.org/10.1016/j.earscirev.2012.08.002

Morley RJ, Bui VD, Nguyen TT, Kullman AJ, Bird RT, Nguyen HC (2019) High-resolution Palaeogene sequence stratigraphic framework for the Cuu Long Basin, offshore Vietnam, driven by climate change and tectonics, established from sequence biostratigraphy. Palaeogeogr Palaeoclimatol Palaeoecol 530:113–135. https://doi.org/10.1016/j.palaeo.2019.05.010

Morley RJ, Morley HP (2013) Mid Cenozoic freshwater wetlands of the Sunda region. J Limnol 72(s2):18–35. https://doi.org/10.4081/jlimnol.2013.S2.E2

Morley RJ, Swiecicki T, Pham DTT (2011) A sequence stratigraphic framework for the Sunda region, based on integration of biostratigraphic, lithological and seismic data from Nam Con Son Basin, Vietnam, Indonesian Petroleum Association (IPA), Jakarta, IPA11-G-002.

Morton A (2007) The role of heavy mineral analysis as a geosteering tool during drilling of high-angle wells. In: Mange MA, Wright DT (eds) Heavy minerals in use. Developments in Sedimentology. https://doi.org/10.1016/S0070-4571(07)58044-1

Morton AC, Hallsworth CR (1994) Identifying provenance-specific features of detrital heavy mineral assemblages in sandstones. Sed Geol 90:241–256. https://doi.org/10.1016/0037-0738(94)90041-8

Nemchin AA, Cawood PA (2005) Discordance of the U-Pb system in detrital zircons: implication for provenance studies of sedimentary rocks. Sed Geol 182:143–162. https://doi.org/10.1016/j.sedgeo.2005.07.011

Nguyen DC, Tan MT, Tran VX, Tran NH (2019) Oligocene combination/stratigraphic traps and their reservoir quality in Cuu Long basin, offshore Vietnam. Petrovietnam Journal 6:30–40. https://doi.org/10.25073/petrovietnam%20journal.v6i0.179

Nguyen HH, Carter A, Van Hoang L, Vu ST (2018) Provenance, routing and weathering history of heavy minerals from coastal placer deposits of southern Vietnam. Sed Geol 373:228–238. https://doi.org/10.1016/j.sedgeo.2018.06.008

Nguyen TT, Nguyen DT (1995) Petroleum geology of the Nam Con Son Basin. Geol. Soc Malaysia, Bulletin 37:1–11. https://doi.org/10.7186/bgsm37199501

Nguyen TTB, Satir M, Siebel W, Chen F (2004) Granitoids in the Dalat zone, southern Vietnam: age constraints on magmatism and regional geological implications. Int J Earth Sci 93:329–340. https://doi.org/10.1007/s00531-004-0387-6

Nguyen VL, Ta TKO, Saito Y (2010) Early Holocene initiation of the Mekong River delta, Vietnam, and the response to Holocene sea-level changes detected from DT1 core analyses. Sed Geol 230:146–155. https://doi.org/10.1016/j.sedgeo.2010.07.006

Nie J, Ruetenik G, Gallagher K, Hoke G, Garzione CN, Wang W, Stockli D, Hu X, Wang Z, Wang Y (2018) Rapid incision of the Mekong River in the middle Miocene linked to monsoonal precipitation. Nat Geosci 11:944–948. https://doi.org/10.1038/s41561-018-0244-z

Nong AT, Hauzenberger CA, Gallhofer D, Dinh SQ (2021) Geochemistry and zircon U-Pb geochronology of Late Mesozoic igneous rocks from SW Vietnam–SE Cambodia: Implications for episodic magmatism in the context of the Paleo-Pacific subduction. Lithos 390:106101. https://doi.org/10.1016/j.lithos.2021.106101

Pearce NJG, Perkins WT, Westgate JA, Gorton MP, Jackson SE, Neal CR, Chenery SP (1997) A Compilation of New and Published Major and Trace Element Data for NIST SRM 610 and NIST SRM 612 Glass Reference Materials. Geostand Newsl 21:115–144. https://doi.org/10.1111/j.1751-908X.1997.tb00538.x

Quang CD (2013) Tham NT (2013) Determining the age of Sequence G, Block 15–1/05 in Cuu Long basin and the relationship between palynological assemblages and sedimentary depositional cycles. Dau Khi so 12:14–19 ((**in Vietnamese**))

Quek LX, Lee T-Y, Ghani AA, Lai Y-M, Roselee MH, Lee H-Y, Iizuka Y, Lin Y-L, Yeh M-W, Amran MA (2021) Tracing detrital signature from Indochina in Peninsular Malaysia fluvial sediment: Possible detrital zircon recycling into West Borneo Cenozoic sediments. J Asian Earth Sci 218:104876. https://doi.org/10.1016/j.jseaes.2021.104876

Racey A, Duddy I, Love M (1997) Apatite fission track analysis of Mesozoic red beds from northeastern Thailand and western Laos. The International Conference on Stratigraphy and Tectonic Evolution of Southeast Asia and the South Pacific, Bangkok, Thailand, pp 200–209

Rangin C, Huchon P, Le Pichon X, Bellon H, Lepvrier C, Roques D, Hoe ND, Van Quynh P (1995) Cenozoic deformation of central and south Vietnam. Tectonophysics 251:179–196. https://doi.org/10.1016/0040-1951(95)00006-2

San NT, Hoang CM, Hoan PK (2013) Palaeogene sediment complex geological factors impacting on its reservoir quality and hydrocarbon potential. Petrovietnam Journal 10:8–17 (http://pvj.com.vn/index.php/TCDK/article/view/706)

Schmidt WJ, Handschy JW, Hoang BH, Morley CK, Tung NT, Tuan NQ (2021) Structure and tectonics of a Late Jurassic, arcuate fold belt in the Ban Don Group. Southern Vietnam Tectonophysics 817:229040. https://doi.org/10.1016/j.tecto.2021.229040

Schmidt WJ, Hoang BH, Handschy JW, Hai VT, Cuong TX, Tung NT (2019) Tectonic evolution and regional setting of the Cuu Long Basin. Vietnam Tectonophysics 757:36–57. https://doi.org/10.1016/j.tecto.2019.03.001

Schmidt WJ, Nguyen VQ, Pham HL (2003) Tectonic development of the Cuu Long Basin, Vietnam. Proceedings of the Science Conference on 25th Anniversary of the Vietnam Petroleum Institute, pp 87–104

Sevastjanova I, Clements B, Hall R, Belousova EA, Griffin WL, Pearson N (2011) Granitic magmatism, basement ages, and provenance indicators in the Malay Peninsula: insights from detrital zircon U-Pb and Hf-isotope data. Gondwana Res 19:1024–1039. https://doi.org/10.1016/j.gr.2010.10.010

Shellnutt JG, Lan C-Y, Van Long T, Usuki T, Yang H-J, Mertzman SA, Iizuka Y, Chung S-L, Wang K-L, Hsu W-Y (2013) Formation of Cretaceous Cordilleran and post-orogenic granites and their microgranular enclaves from the Dalat zone, southern Vietnam: tectonic implications for the evolution of Southeast Asia. Lithos 182–183:229–241. https://doi.org/10.1016/j.lithos.2013.09.016

Sircombe KN (2004) AgeDisplay: an EXCEL workbook to evaluate and display univariate geochronological data using binned frequency histograms and probability density distributions. Comput Geosci 30:21–31. https://doi.org/10.1016/j.cageo.2003.09.006

Sláma J, Košler J, Condon DJ, Crowley JL, Gerdes A, Hanchar JM, Horstwood MSA, Morris GA, Nasdala L, Norberg N, Schaltegger U, Schoene B, Tubrett MN, Whitehouse MJ (2008) Plešovice zircon — A new natural reference material for U-Pb and Hf isotopic microanalysis. Chem Geol 249:1–35. https://doi.org/10.1016/j.chemgeo.2007.11.005

Suggate SM, Cottam MA, Hall R, Sevastjanova I, Forster MA, White LT, Armstrong RA, Carter A, Mojares E (2014) South China continental margin signature for sandstones and granites from Palawan, Philippines. Gondwana Res 26:699–718. https://doi.org/10.1016/j.gr.2013.07.006

Swiecicki T, Maynard K (2009) Geology and sequence, stratigraphy of block 06/94, Nam Con Son Basin, Offshore Vietnam. South East Asia Petroleum Exploration Society (SEAPEX) Conference, Singapore

Ta TKO, Nguyen VL, Saito Y, Gugliotta M, Tamura T, Nguyen TML, Truong MH, Bui TL (2021) Latest Pleistocene to Holocene stratigraphic record and evolution of the Paleo-Mekong incised valley. Vietnam Mar Geol 433:106406. https://doi.org/10.1016/j.margeo.2020.106406

Ta TKO, Nguyen VL, Tateishi M, Kobayashi I, Tanabe S, Saito Y (2002) Holocene delta evolution and sediment discharge of the Mekong River, southern Vietnam. Quatern Sci Rev 21:1807–1819. https://doi.org/10.1016/S0277-3791(02)00007-0

Tanabe S, Ta TKO, Nguyen VL, Tateishi M, Kobayashi I, Saito Y (2003) Delta evolution model inferred from the Holocene Mekong Delta, southern Vietnam. In Sidi FH, Nummedal D, Imbert P, Darman H, Posamentier HW (eds) Tropical Deltas of Southeast Asia-sedimentology, stratigraphy, and petroleum geology, SEPM Special Publication 76. https://doi.org/10.2110/pec.03.76.0175

Tang X, Yang S, Hu S (2020) Provenance of the Paleogene sediments in the Pearl River Mouth Basin, northern South China Sea: Insights from zircon U-Pb and fission track double dating. J Asian Earth Sci 200:104494. https://doi.org/10.1016/j.jseaes.2020.104494

Tham NT, Van Su N (2016) Neogene calcareous nannofossils from the Nam Con Son Basin, offshore Vietnam. J Nannoplankton Res 36:151–160

Thanh NT, Cuong DH, Stattegger K, Dung BV, Yang S, Chi NTK, Tung NX, Van Tinh N, Nga NT (2021) Depositional sequences of the Mekong river delta and adjacent shelf over the past 140 kyr, southern Vietnam. J Asian Earth Sci 206:104634. https://doi.org/10.1016/j.jseaes.2020.104634

Tran LD, Phung DH (2007) Cuu Long sedimentary basin and petroleum resources. The Petroleum Geology and Resources of Vietnam. In: The Science and Technology Publishing House, 1st ed

Tuan NQ, Van Tri T (2016) Seismic interpretation of the Nam Con Son basin and its implication for the tectonic evolution. Indones J Geosci 3:127–137. https://doi.org/10.17014/ijog.3.2.127-137

Van Hattum M, Hall R, Pickard A, Nichols G (2013) Provenance and geochronology of Cenozoic sandstones of northern Borneo. J Asian Earth Sci 76:266–282. https://doi.org/10.1016/j.jseaes.2013.02.033

Vermeesch P (2013) Multi-sample comparison of detrital age distributions. Chem Geol 341:140–146. https://doi.org/10.1016/j.chemgeo.2013.01.010

Vermeesch P (2018) IsoplotR: a free and open toolbox for geochronology. Geosci Front 9:1479–1493. https://doi.org/10.1016/j.gsf.2018.04.001

Vermeesch P, Resentini A, Garzanti E (2016) An R package for statistical provenance analysis. Sed Geol. https://doi.org/10.1016/j.sedgeo.2016.01.009

Waight T, Fyhn MB, Thomsen TB, Van Tri T, Nielsen LH, Abatzis I, Frei D (2021) Permian to Cretaceous granites and felsic volcanics from SW Vietnam and S Cambodia: Implications for tectonic development of Indochina. J Asian Earth Sci 219:104902. https://doi.org/10.1016/j.jseaes.2021.104902

Wang C, Liang X, Foster DA, Tong C, Liu P, Liang X, Zhang L (2019) Linking source and sink: Detrital zircon provenance record of drainage systems in Vietnam and the Yinggehai-Song Hong Basin, South China Sea. GSA Bull 131:191–204. https://doi.org/10.1130/B32007.1

Wang C, Liang X, Xie Y, Tong C, Pei J, Zhou Y, Jiang Y, Fu J, Dong C, Liu P (2014) Provenance of upper Miocene to Quaternary sediments in the Yinggehai-Song Hong Basin, south China sea: Evidence from detrital zircon U-Pb ages. Mar Geol 355:202–217. https://doi.org/10.1016/j.margeo.2014.06.004

Wang C, Wen S, Liang X, Shi H, Liang X (2018) Detrital zircon provenance record of the Oligocene Zhuhai Formation in the Pearl River Mouth Basin, northern South China Sea. Mar Pet Geol 98:448–461. https://doi.org/10.1016/j.marpetgeo.2018.08.032

Wang L, Shen L, Liu C, Ding L (2020) Evolution of the paleo-Mekong River in the Early Cretaceous: Insights from the provenance of sandstones in the Vientiane Basin, central Laos. Palaeogeogr Palaeoclimatol Palaeoecol 545:109651. https://doi.org/10.1016/j.palaeo.2020.109651

Xu C, Shi H, Barnes CG, Zhou Z (2016) Tracing a late Mesozoic magmatic arc along the Southeast Asian margin from the granitoids drilled from the northern South China Sea. Int Geol Rev 58:71–94. https://doi.org/10.1080/00206814.2015.1056256

Xue Z, Liu JP, DeMaster D, Van Nguyen L, Ta TKO (2010) Late Holocene evolution of the Mekong subaqueous delta, southern Vietnam. Mar Geol 269:46–60. https://doi.org/10.1016/j.margeo.2009.12.005

Yan Y, Yao D, Tian Z, Huang C, Chen W, Santosh M, Yumul GP Jr, Dimalanta CB, Li Z (2018) Zircon U-Pb chronology and Hf isotope from the Palawan-Mindoro block, Philippines: implication to provenance and tectonic evolution of the South China Sea. Tectonics 37:1063–1076. https://doi.org/10.1002/2017TC004942

Yu M, Yan Y, Huang CY, Zhang X, Tian Z, Chen WH, Santosh M (2018) Opening of the South China Sea and upwelling of the Hainan plume. Geophys Res Lett 45:2600–2609. https://doi.org/10.1002/2017GL076872

Zhang G-L, Luo Q, Zhao J, Jackson MG, Guo L-S, Zhong L-F (2018) Geochemical nature of sub-ridge mantle and opening dynamics of the South China Sea. Earth Planet Sci Lett 489:145–155. https://doi.org/10.1016/j.epsl.2018.02.040

Zhang P, Najman Y, Mei L, Millar I, Sobel ER, Carter A, Barfod D, Dhuime B, Garzanti E, Govin G (2019) Palaeodrainage evolution of the large rivers of East Asia, and Himalayan-Tibet tectonics. Earth Sci Rev 192:601–630. https://doi.org/10.1016/j.earscirev.2019.02.003

Zhong L-F, Cai G-Q, Koppers AA, Xu Y-G, Xu H-H, Gao H-F, Xia B (2018) $^{40}Ar/^{39}Ar$ dating of oceanic plagiogranite: Constraints on the initiation of seafloor spreading in the South China Sea. Lithos 302:421–426. https://doi.org/10.1016/j.lithos.2018.01.018

Zimmermann S, Mark C, Chew D, Voice PJ (2018) Maximising data and precision from detrital zircon U-Pb analysis by LA–ICPMS: The use of core–rim ages and the single-analysis concordia age. Sed Geol 375:5–13. https://doi.org/10.1016/j.sedgeo.2017.12.020